Development of Embedded Fiber *Bragg* Grating Sensors using 3D Printing Technique

Rita Trovão Pereira de Lima
Integrated Master's in Engineering Physics
Departamet of Physics and Astronomy
2017

Supervisor
Orlando José dos Reis Frazão, Auxiliar Professor, Faculty of Sciences of University of Porto and Senior Researcher, INESC-TEC

Co-Supervisor
Susana Ferreira de Oliveira Silva, Auxiliar Researcher, Faculty of Sciences of University of Porto

All modifications determined by the Jury, and onlly those, were made.

The chairman of the Jury,

Porto, _____/_____/_____

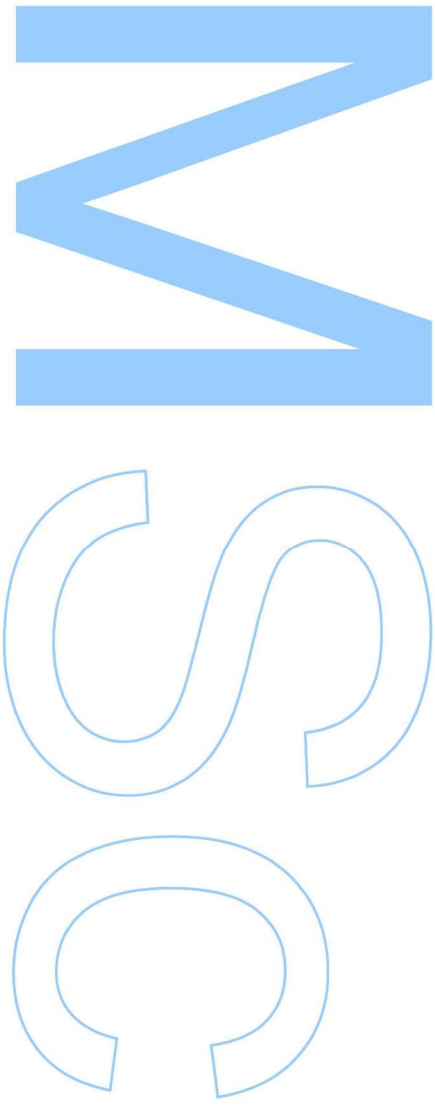

Acknowledgements

This work would not be possible without the contribution and help of many people who support me during the development of this thesis. I wish to thank all of them however, it is only possible to mention some.

This thesis would not have been possible without the support and encouragement of Dr. Orlando Frazão, my supervisor, and Dra. Susana Silva, my co-supervisor. Their dedication, professionalism and enthusiasm were fundamental to improve my academic record. Their work ethic inspired me to succeed in every ways. To them my sincere gratitude for all the opportunities.

I am thankful to the Center for Applied Photonics of INESC-TEC colleagues for welcoming me and for the opportunity to work for the first time in a professional environment, especially to Hugo Santos, for the assistance and availability in the access to the 3D printer used to develop my research work. I am very grateful for all the support and good will.

Also, to the CORAL project, financed by FCT - Fundação para a Ciência e Tecnologia (Portuguese Foundation for Science and Technology) and by ERDF (European Regional Development Fund) through: COMPETE Program (Operational Program for Competitiveness) within project FCOMP-01-0124-FEDER-037281; ON.2 - O Novo Norte (Northern Portugal Regional Operational Program).

I would like to thank my amazing friends for all the friendship and support, the fruitful discussions, optimism and shared experiences. A special thanks to Rúben Alves, for all the patience and humility. I am so grateful and I wish them all the best.

A very special thanks to Davide for the profitable discussions, the help to deal with difficult situations and for all the love, happiness and unconditional support during this journey.

I would like to thank my family for supporting my decisions: My brother, Gabriel, for all the laughs and joy in the most difficult times; My mother, Maria José, for the unconditional love, strength and courage, to do what only a few would dare; And to my grandfather Carlos, who has always believed in me and in what I am capable of.

Abstract

This thesis explores the development and characterization of optical fiber sensors based on Fiber *Bragg* Gratings (*FBG*) embedded on 3D printed polymer. The main goal is to develop and design a new sensor's housing, by implementing the 3D printing technique, thus improving the optical sensor protection without compromising its response. With this, it is possible to implement the sensors and profit from its sensitivity in harsh environments. In order to prove this innovative concept, an optical fiber pressure sensor and an optical fiber accelerometer were assembled and characterized. Both based on *FBGs* embedded in 3-Dimensions (3D) printed polymer.

This dissertation starts with a brief introduction presenting the motivation, explaining how the work is organized and some outputs achieved. Followed by an introduction on 3D printing technique, Fiber *Bragg* Gratings and some applications. The developed optical sensors are presented in two chapters: optical fiber pressure sensor and optical fiber accelerometer. In these two chapters, the fabrication process is described and the characterization results are presented for both sensors. The optical fiber pressure sensor was developed in a cantilever structure where the *FBG* was embedded. A pressure and a vibration characterization were performed, to assess the optical sensor's response and the influence of the printed polymer. The optical fiber accelerometer was developed in three configurations: 1D, 2D and 3D. The sensor head was also a cantilever structure implemented in a cubic design. A displacement and a vibration characterization were performed for all configurations, and the concept of acceleration variation was proved by assembling the cubic structure, for the three configurations presented.

In the end, the main conclusions are presented, some results are discussed and new possibilities are explored along with the suggested future work.

Keywords: Optical fiber sensors, fiber *Bragg* gratings, 3D printing technique, optical sensors housing.

Resumo

Esta tese explora o desenvolvimento e caracterização de sensores em fibra ótica baseados em redes de *Bragg* (*FBG*) incorporadas em material polimérico impresso, utilizando a técnica de impressão em 3-Dimensões (3D). O objetivo principal consistiu em desenvolver e optimizar um novo conceito de encapsulamento de sensores óticos, implementando a técnica de impressão 3D, melhorando assim a proteção conferida ao sensor ótico sem comprometer a sua leitura e sensibilidade. Desta forma, é possível implementar o sensor *FBG* e beneficiar da sua elevada sensibilidade, em ambientes hostis. De modo a provar este conceito, um sensor de pressão em fibra ótica e um acelerómetro em fibra ótica foram desenvolvidos e caraterizados. Ambos, baseados em *FBGs* incorporados no material polimérico impresso através da técnica de impressão 3D.

A dissertação começa com uma breve introdução onde é apresentada a motivação, a organização do trabalho desenvolvido e alguns *outputs*. Seguidamente, um estado da arte, que explora a técnica de impressão 3D e sensores de *Bragg* juntamente com possíveis aplicações, é também apresentado. Os sensores em fibra ótica desenvolvidos estão divididos em dois capítulos: sensor de pressão em fibra ótica e acelerómetro em fibra ótica, onde o processo de fabricação é descrito e os resultados obtidos na caracterização são apresentados. O sensor de pressão foi desenvolvido numa estrutura em cantiléver, onde a rede de *Bragg* foi incorporada. Uma caracterização em pressão e vibração foi executada, de forma a avaliar a resposta do sensor ótico e a influência do material polimérico na sensibilidade caraterística. O acelerómetro foi desenvolvido em três configurações: 1D, 2D e 3D. A rede de *Bragg* foi também incorporada numa estrutura em cantiléver e, esta foi implementada na face de uma estrutura cúbica. Uma caracterização em deslocamento e vibração foi realizada para as três configurações e, o conceito de variação de aceleração com a variação de posição foi comprovado, também para as três configurações.

No final, as principais conclusões são apresentadas, alguns resultados são discutidos e novas aplicações são exploradas, juntamente com o trabalho futuro sugerido.

Palavras-Chave: Sensores em fibra ótica, sensores de Bragg, técnica de impressão 3D, encapsulamento de sensores óticos.

Contents

Acknowledgements iii

Abstract iv

Resumo v

List of Tables viii

List of Figures xi

1 Introduction 1

1.1 Motivation 1

1.2 Objectives 3

1.3 Outputs 3

2 State of the Art: The 3D Printing Technique 4

2.1 The 3D Printing Technique 5

2.2 3D Printing Methods 6

3 State of the Art: Fiber Bragg Grating Sensors 11

3.1 Fiber Bragg Grating Sensors 12

3.2 Brief Review of Sensing Applications 15

3.2.1 Fiber Optic Accelerometer 15

3.2.2 Pressure Sensor 16

4 Optical Fiber Pressure Sensor **20**

4.1 Simulation and Experimental Configuration 20

4.2 Experimental Results 22

4.2.1 Pressure Characterization 24

4.2.2 Vibration Characterization 26

4.3 Discussions 29

5 Optical Fiber Accelerometer **30**

5.1 Simulation and Experimental Configuration 31

5.2 Experimental Results 33

5.2.1 1D Configuration Characterization 33

5.2.2 2D Configuration Characterization 35

5.2.3 3D Configuration Characterization 39

5.3 Discussions 43

6 Final Conclusions and Future Work **45**

A Cantilever Structure **48**

B Optical Fiber Pressure Sensor: Design and Simulations **53**

References **55**

List of Tables

2.1 Resume of 3D printing methods and respective printing materials. 10

5.1 Fit results from displacement characterization. 41

5.2 Determined results from vibration characterization. 42

List of Figures

2.1 The first 3D printer, built by Charles Hull in 1983. 4

2.2 Extrusion Deposition apparatus. 6

2.3 Representative setup of the Binding of Granular Materials method. 7

2.4 Lamination method apparatus. 7

2.5 Photo-polymerization method apparatus. 8

2.6 Representative scheme of Metal wire process. 9

3.1 Representative scheme of a FBG and the variation of the core's refractive index [1]. 12

3.2 Results obtained in the analysis of a FBG centered in 1546.2 nm, in reflection and transmission [1]. 13

3.3 Characterization of a FBG on temperature and strain. 14

3.4 Diagram of a FBG accelerometer design. 16

3.5 Proposed setup for sensing finger movements [2]. 17

3.6 Example of a fiber optic pressure sensor, where is illustrated both optical fibers, for the incident and the reflected signal by the diaphragm [3]. 17

3.7 Schematics of the fiber Bragg probe configuration [4]. 18

3.8 The setup used to preform the mechanical characterization with arbitrary waveforms [4]. 19

4.1 Pressure sensor designed: sensor's base (black) and head (blue). 21

4.2 Strain simulation to assess the behavior of the sensor head under applied pressure, approximately $5kPa$. 21

4.3 Main setup for both analysis. 22

4.4 Fabricated optical fiber pressure sensor prototype. 23

4.5 Reflection spectrum of the sensor, before (black) and after (green) the printing process with none applied pressure and, after the printing process with applied pressure (red). 23

4.6 *Bragg* wavelength values of seven consecutive loads and unloads for $100g$ steps. 24

4.7 *Bragg* wavelength shift of *Bragg* wavelength mean values as a function of pressure. 25

4.8 *Bragg* wavelength variation for twenty consecutive measures of $0g$ and $100g$ loads. 26

4.9 Reflection spectra for optic(left) and electric(right) analysis of the selected frequencies: $1.5Hz$, $2Hz$ and $5Hz$, respectively up bottom, left right. 27

4.10 FFT representation of the signal reproduced by the assembled sensor, (a)$1.5Hz$, (b)$2Hz$ and (c)$5Hz$. 28

5.1 Fiber optic accelerometer simulation and design: a cubic structure with a cantilever configuration placed. 31

5.2 Strain simulation to assess the most sensitive spot under applied force. . . . 32

5.3 (a) 3D printed part for the 1D optical fiber accelerometer and (b) its simulation. 33

5.4 Results of displacement characterization. 34

5.5 Vibration characterization: Position, velocity and acceleration determined. . . 34

5.6 Variation of amplitude as a function of time. 35

5.7 (a) one 3D printed part for 2D optical fiber accelerometer and (b) its simulation. 36

5.8 Results of displacement characterization for the first printed sensor: (a) *Bragg* wavelength and (b) optical power behavior. 36

5.9 Results of displacement characterization for the second printed sensor: (a) *Bragg* wavelength and (b) optical power behavior. 37

5.10 Results of vibration characterization for both printed sensors: (a) first and (b) second sensor. 38

5.11 Variation of amplitude as a function of time. 38

5.12 3D optical fiber accelerometer: (a) one of the printed parts and (b) its simulation. 39

5.13 Results of displacement characterization for (a,b) first, (c,d) second and (e,f) third printed sensors. 40

5.14 Results of vibration characterization for (a) first, (b) second and (c) third printed sensors. 41

5.15 Acceleration variation sensing. 42

A.1 Two cantilevers shaped sensors, printed with embedded *FBGs*. 48

A.2 Displacement characterization. 49

A.3 Temperature characterization. 50

A.4 Vibration characterization. 50

A.5 Displacement characterization: (a) *Bragg* wavelength shift during displacement characterization, dummy fiber on the left, (b) Wavelength shift in function of displacement and (c) Optical power in function of displacement. 51

A.6 Vibration characterization. 52

B.1 Strain simulation results for two cantilever structure: (a) frontal view and (b) bottom view. 53

B.2 Strain simulation results for four cantilever structure: (a) frontal view and (b) bottom view. 54

Chapter 1

Introduction

1.1 Motivation

The study of a suitable housing for an optical fiber sensor is a wide field of expertise, not only due to the need of protecting the optical sensor, but also due to its applications in the measuring environment. A viable sensor housing should not interfere with the response nor with the sensitivity of the sensor. The characteristics of the sensor must remain unchanged, by adapting the housing to the possible applications.

Many studies have been developed within optical fiber sensors, exploring and testing different optical elements such as fiber Bragg gratings (*FBGs*), intensity sensors and Fabry-Perot technique [5, 6]; under several physical parameters, such as strain, temperature, vibration, pressure and displacement, always with promising results in their application [7, 8, 9, 10]. Not only due to the optical fiber properties, which are remarkable in different areas, but also due to structure endurance.

In particular, *FBG*, which consists on a periodic change on the optical fiber core's refractive index, reveals good sensitivity and a well known behavior, which are both advantageous features in a sensor.

The applications of 3D printing technique are remarkable and are considered promising and revealing in several areas [11, 12, 13]. This technique proved to be a good solution for an optical fiber sensor housing. Despite the advantages, in particular the fact that the housing does not interfere with the sensor's reading and that is customizable, there are some challenges. Adjusting each area of expertise to a suitable optical element and to a corresponding housing is one of the challenges, in order to promote a sustainable signal processing and create an easy interface between the system and the user. According

to that, the study of different geometries is necessary to adjust and improve the sensor's housing.

By introducing 3D printing technique as a solution to the housing problem, it is possible to apply optical fiber sensors in specific and hostile environments, without compromising the expected performance of the optical sensor [14].

This dissertation is divided in five chapters with the following structure:

The first chapter is organized to describe the research work developed, its context and relevance on the scientific field. It presents the motivation, proposed objectives, document structure and achieved outputs.

In the second chapter, the *FBG* sensor is explored along with its working principle and characteristic spectra. A brief review of sensing applications is presented, focusing on the performance of FBG as optical sensor implemented on fiber optic accelerometers and pressure sensors.

The third chapter introduces the 3D printing technique, some historical facts and the different 3D printing methods that are normally used are also presented. The advantages and disadvantages of these methods are explored, as well as the different printing materials.

Chapter 4 explores the concept of embedding a fiber optic sensor in a 3D printed polymer. The developed structure is designed to perform acceleration measurements, based on the deformation of the sensor that is embedded. Established on this idea, a fiber optic accelerometer is assembled, in a cubic structure, and its characteristics are studied, mainly the possibility to monitoring movements. The registered results are presented and discussed, both, from optical and electrical analysis, along with its conclusions.

Chapter 5 presents another structure assembled by the same procedure. A fiber optic pressure sensor based on a FBG embedded on a cantilever structure, fabricated through the 3D printing technique, is presented. The sensitivity of the sensor is studied, along with its ability of sensing low frequencies. Again, was performed an electrical and optical analysis, also to assess the best signal processing system.

The final chapter contains the conclusions and a brief discussion about the possible applications of the developed work. Finally, some future work is presented and discussed.

1.2 Objectives

The main goals of this thesis are the study of new fiber optical sensors based on FBG, for acceleration and pressure measurements and, the assessment of a different housing for the optical sensor, mainly embedded in a 3D printed polymer of polylactic acid (PLA). The application of the cantilever configuration in the produced structures is also a goal, due to the high sensitivity associated with the setting. The main objectives of this dissertation are:

- Study of new configurations for acceleration and pressure measurements.
- Analyze new materials and techniques for optical sensors housing.
- Investigation of the reliability of these new devices in biomedical environment.

1.3 Outputs

Rita Lima, H. M. Santos, S. O. Silva and O. Frazão, ”Fiber Bragg grating embedded in polymer 3D printed material for acceleration measurement”, In DCE 17 - 2nd Doctoral Congress in Engineering, Porto, Portugal, June 8-9, 2017.

Rita Lima, R. Tavares, S. O. Silva, P. Abreu, Maria T. Restivo and O. Frazão, ”Fiber Bragg grating embedded in polymer 3D printed material for acceleration measurement”, In AOP 2017 - III International Conference on Applications of Optics and Photonics, Faro, Portugal, May 8-12, 2017.

Rita Lima, R. Tavares, S. O. Silva, P. Abreu, Maria T. Restivo and O. Frazão, ”Fiber Bragg grating sensor based on cantilever structure embedded in polymer 3D printed material”, In OFS-25 - The 25th International Conference on Optical Fiber Sensors, Jeju, Korea, April 24-28, 2017.

Rita Lima, S. O. Silva and O. Frazão, ”Fiber Bragg grating embedded in polymer 3D printed material for acceleration measurement”, In II Jornadas de Engenharia Física, Porto, Portugal, March 27.

Rita Lima, S. O. Silva and O. Frazão, ”Fiber Bragg grating embedded in polymer 3D printed material for pressure measurement”, In *IEEE Sensors Journal*, 2017. (*submitted*)

Chapter 2

State of the Art: The 3D Printing Technique

The 3D printing process was invented in the early 1980s by Charles Hull [15], and was described as stereolithography or, the printing of successive layers of material to produce a three-dimensional object (layer-by-layer process). The 3D printer can print different materials, but the most used are thermopolymeric or metallic (aluminum, stainless steel and titanium 6.4 are the most common), powder or filament. The printing material is slowly molded by the extrusion process. This process lies in making the printing material plastic, malleable, in order to shape it, forming the desired object on a layer-by-layer basis [11, 12]. The first 3D printer (see figure 2.1.) was built and the 3D printing concept was proved to be possible in 1983 by its inventor. A review of this technique will be presented in this chapter, along with the several existing printing methods. The methods and some advantages and disadvantages will also be discussed.

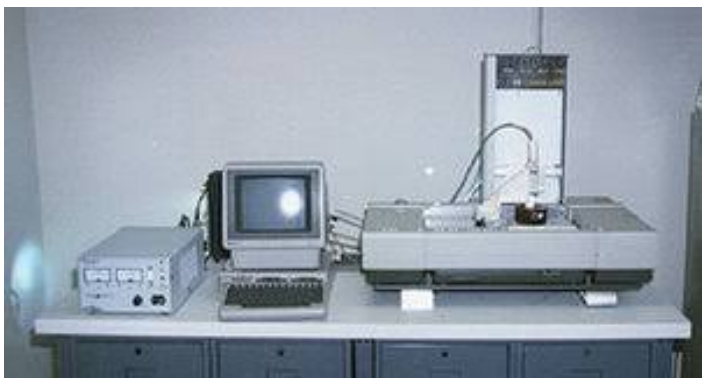

Figure 2.1: The first 3D printer, built by Charles Hull in 1983.

2.1 The 3D Printing Technique

The applications of the 3D printing technique are considered groundbreaking in several areas, from optics to medicine [11, 12, 13]. This process, also known as an Additive Manufacturing (AM) procedure, is used to produce 3D objects in a layer-by-layer process, where successive layers of material are displayed under computer control to form the final object [16, 17]. This technique diverges from a traditional ink-based printing process which produces a 2D object. All 3D printers need a combined software, commonly *SolidWorks* or *3D-CAD* (among others), that provides a global view of the final 3D object and implements a sectioning of the same object, that will be read and executed by the printer. The process resolution is also an important component to be taken in consideration, since it defines the minimum thickness of each layer and, therefore, how detailed will be the final product. Considering three dimensions: two planar dimensions (X e Y) and the Z dimension, which characterizes the 3D process, it is possible to distinguish between horizontal and vertical resolutions, and these are controlled by different mechanisms:

- *Horizontal Resolution*: is characterized by the slightest movement that the head extruder can make on X and Y axis, in the printing of a layer. The smaller the value, the greater the detail that the printer produces.

- *Vertical Resolution*: described as the layer thickness or height, is the minimal thickness that the printer produces in one pass, by layer. The smaller the thickness of the layer, more polished will be the printed surface.

One should note that the printing process will take longer as the layer thickness decreases, and that each printing method, as well as the printer itself has an associated resolution (vertical and horizontal). And that, the printer and the method should be chosen taking into account the final object. The printer resolution usually is represented in dots per inches or in micrometers (μm), and depends on the printing method and on the desired final product. Typical layer thickness is about 100μm, some printers can produce layers around 16μm.

2.2 3D Printing Methods

There are mainly six printing methods. The differences between processes are the materials used and, some nuances of the deposition technique. Some methods soften or melt the material to build the final product, while others cure liquid materials. The mainly six methods are the following [16, 17]:

Extrusion Deposition

This method, also known as Fused Deposition Modeling (FDM), results from an automatic polymeric foil hot air system, hot-melt attaching and automatic stopper deposition. The object to print is produced by extrusion of small amounts of material, which solidify immediately on contact with the air, forming successive layers. A filament of thermoplastic or a metal wire is stored in a coil and is released to provide the printer extruder.

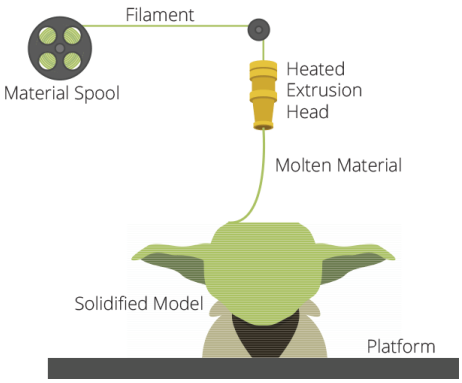

Figure 2.2: Extrusion Deposition apparatus.

Binding of Granular Materials

This method consists on the selective fusing of materials in a granular bed. Parts of the layer are fused, then another layer of granules is added and the process is repeated until the final object is completed. This process doesn't use melted material to support overhangs and thin walls in the part that is in production, which reduces the need for auxiliary temporary supports for the workpiece.

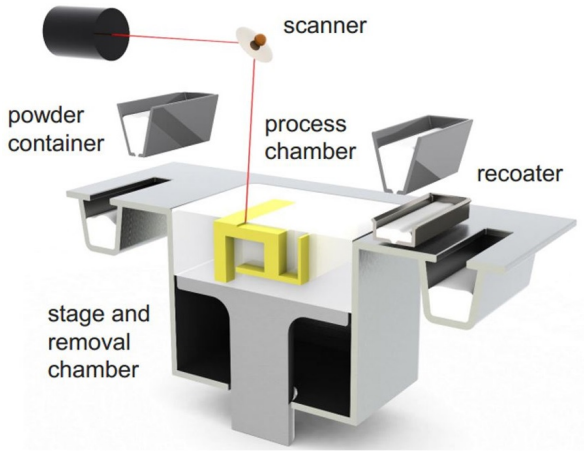

Figure 2.3: Representative setup of the Binding of Granular Materials method.

Lamination Method

In some 3D printers, the paper can be used as building material, resulting in a low-cost printing. This process introduces printers that cut cross sections of a special adhesive coated paper, using a carbon dioxide laser and then laminate them together (see Figure 2.4). The leaves that are laminated can also be of thin sheets of metal or plastic.

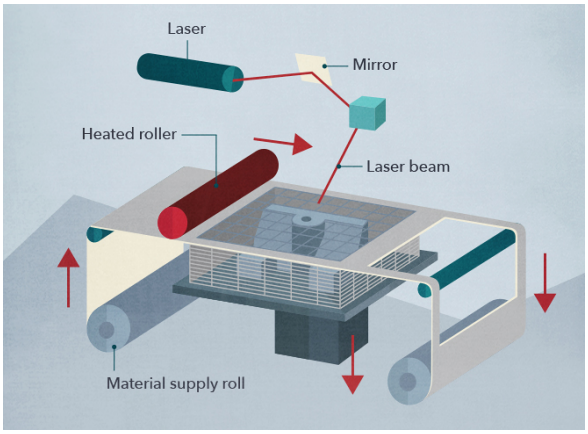

Figure 2.4: Lamination method apparatus.

Many variables can be adjusted to improve this method, such as the blade that cuts the predefined shape, and the pressure to form the prototype.

Photo-polymerization Method

In the photo-polymerization, a small amount of liquid polymer is exposed to a laser, which results in the solidification of liquid polymer exposed. Polymerization occurs when the photo-polymers, which contain chromophores, are exposed to light, otherwise, the addition of molecules, which are photosensitive, is used to react with the solution and start the polymerization. This process of polymerization of monomers leads to cross-linking, which creates a polymer with bonds of the covalent type. When these covalent bonds are formed, the properties of the solution are altered. The build plate moves down and the liquid polymer is again exposed. The process repeats until the final piece is completed.

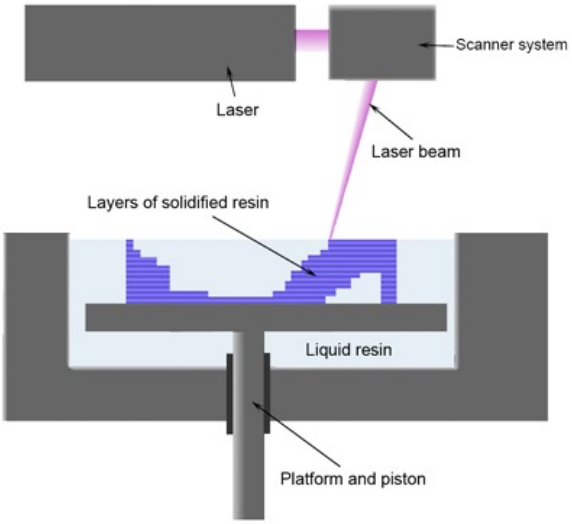

Figure 2.5: Photo-polymerization method apparatus.

Powder Fed Directed Energy Deposition

In this method, is used a high-power laser to melt the printing material (powder), which is provided in the focus of the laser beam. Typically, laser beam travels through the center of the printing head and, is focused by one or more lenses. The printing head is moved up as each layer is completed.
Using the described approach, it is possible to print a variety of materials, including titanium, stainless steel and aluminum. This technique not only allows the production of an entirely new metal part, but also the addition of material to existing parts [18].

Metal Wire Processes

In this process, the laser, which melts the material to print, moves along with the nozzle, which provides the material for the process. This repeats layer by layer until printing is complete. The procedure is controlled by an inert gas, shielding in an open environment (inert gas surrounding the laser) or in a sealed chamber (vacuum chamber). It is possible to use the traditional metal inert gas welding, fixed to the 3D printing stage, for printing materials such as aluminum and steel.

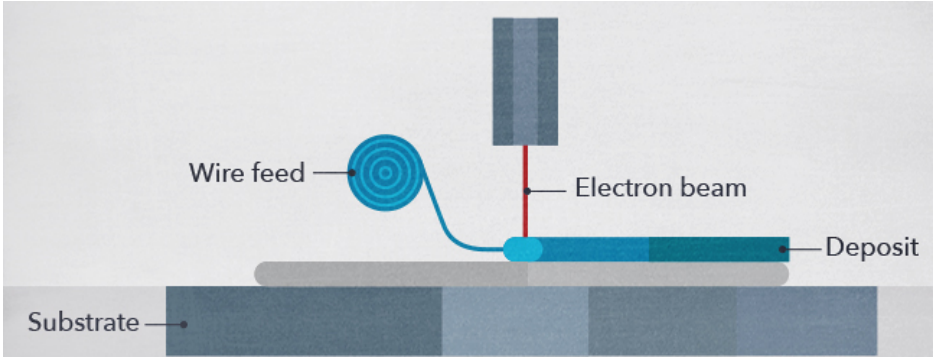

Figure 2.6: Representative scheme of Metal wire process.

In order to promote low-cost equipment, some open-source 3D printers have been outfitted with sensors (mainly Arduino based) and exhibit reasonable metallurgical proprieties from traditionally welding. This idea was first developed at the University of Bath, England, with the ambition of creating a 3D printer that could print its own components, namely the *RepRap Project*, Replicating Rapid Prototyper [19].
Briefly in Table 2.1, there is a resume of each printing method and the respective printing material, commonly used.

Back in 2012, *Berman* [11], reviewed the advantages and applications of 3D printing, comparing it with other technologies. Some of the advantages of this printing technique are the automated manufacturing, the absence of tools or molds, a minimal inventory risk, as there is no unsold products; and the opportunity to recycle wasted material. Also, all products can be easily modified and design through the associated software. In 2013, Schubert *et al.* [12], found this process undeveloped in large scale and outside the engineering area, commending the effort of exploring new fields, such as medicine, in particular ophthalmology, and manufacturing.

Method	**Material**
Extrusion	Thermoplastics Ceramics Eutectic Metals
Photo-Polymerization	Photo-polymer
Binding of Granular Mateials (Powder Bed)	Metal and Titanium Alloys Thermoplastic Ceramics Powder
Lamination	Paper Metal Foil Plastic Film
Powder Fed	Metal Alloy
Metal Wire	Metal Alloy

Table 2.1: Resume of 3D printing methods and respective printing materials.

The applications are extensive, mostly in small productions, due to the cost for large scale productions, such as prototypes, replacement parts, medical applications and mass- customized products. Although, in medium productions, bridge manufacturing revealed to be an assuring application as well. The current limitations of this technique subsist in the, already mentioned, higher costs for large scale production, but the limited strength and resistance to high temperatures are also relevant disadvantages.

Chapter 3

State of the Art: Fiber Bragg Grating Sensors

In the early 1840s, the principle of guiding light by refraction, was first demonstrated by Daniel Colladon and Jacques Babinet. In 1870, Jonh Tyndal wrote about the phenomenon of Total Internal Reflection (TIR) in a brief review of the nature of light [20]. In the beginning of 20th century, new applications began to appear, mainly for internal medical examinations. The first fiberscope was developed by Harold Hopkins and Narinder Kapany in 1953; this device could replace the *"train of lenses"* used in conventional endoscopes [21]. After that event, many followed, for example the development of the gastroscope in 1956. During the development of that application, the first glass-clad fibers were fabricated, by Lawrence E. Curtiss; before this, the clad material was mainly air or low-index oils and waxes [22].

The term *"fiber optics"* emerged in 1960 and, the first working fiber-optic data transmission system was assembled in 1965 by Manfred Börner, a German physicist, which led to the first fiber optic patent [22, 23]. Charles Kao and George Hockham, also in 1965, promote the optical fiber as a practical communication medium, by implementing the idea that the attenuation in fibers was caused by impurities that could be removed, instead of scattering and so, it could be reduced below 20dB [22].

Shortly after, in 1978, the concept of wavelength division multiplexing (WDM) was first published. This technology multiplexes several optic signal shippers into a single optical fiber, by using different wavelengths [24]. In the same year, Ken Hill demonstrated the working principle of the first fiber Bragg grating, fabricated through a visible laser propagating along the fiber core [25]. In addition to these devices, since 1980, fiber optic sensors based in interferometry started to be implemented in several applications. This method was grounded on the Fabry-Perot interferometer principle, that was developed by Charles Fabry and Alfred Perot in 1897 [26]. Later on, other optical fiber devices were developed and

began to emerge.

In this chapter, the FBG, as an optical sensor, is presented and discussed. A brief review of sensing applications is also presented and discussed, especially the fiber optic accelerometer and fiber optic pressure sensor.

3.1 Fiber Bragg Grating Sensors

The *FBG* is a reliable and precise optical fiber sensor, that is possible to be embedded by the printing material, without decreasing the sensor's sensitivity and signal losses. It is possible to embed the chosen optical sensor using the 3D printing technique due to its characteristics, especially due to their size and high temperature resistance (the printing process requires high temperatures) [27]. Hence, it is viable to study and print different housing geometries, embedding the optical element, and testing the obtained signal after the printing process. By comparing it to the previous one and checking how, and how much, the process changed the sensor behavior, it is possible to calibrate the embedded sensor for a future application. Tests, like the ones described, were performed in distinct cases, such as interactive devices, aiming to test the interface with users, and mechanical sensors, to detect defects. The *FBG* sensor is an optical element commonly used in sensing. The FBG consists on a periodic perturbation of the refractive index of the core of an optical fiber. The periodic perturbation is printed in the core, usually using the phase mask technique [5, 28, 1, 29]. The working principle follows the *Bragg* Condition, which relates the Bragg

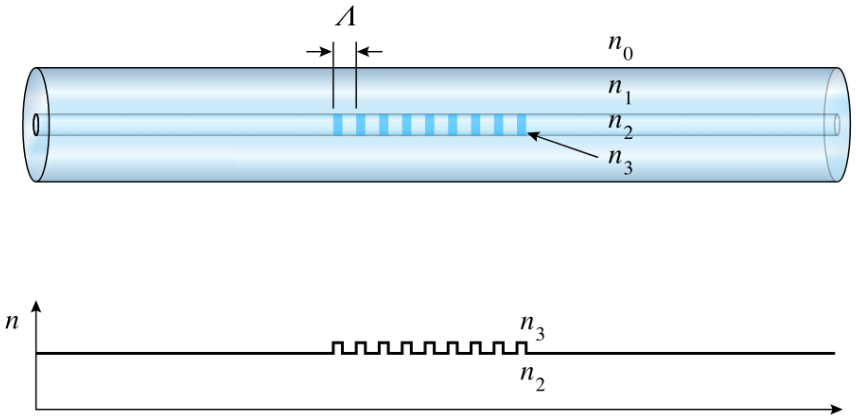

Figure 3.1: Representative scheme of a FBG and the variation of the core's refractive index [1].

wavelength, λ_B, with the effective refractive index, n_{eff} and the grating period, Λ,

$$\lambda_B = 2n_{eff}\Lambda \tag{3.1}$$

The periodic perturbation in the fiber's core works as a mirror, reflecting a specific wavelength, λ_B, and transmitting the remaining wavelength. In this way, it is possible to perform two different measurements, one in reflection and the other in transmission and, obtain to different results, the *Bragg* wavelength and the remaining spectrum, respectively.

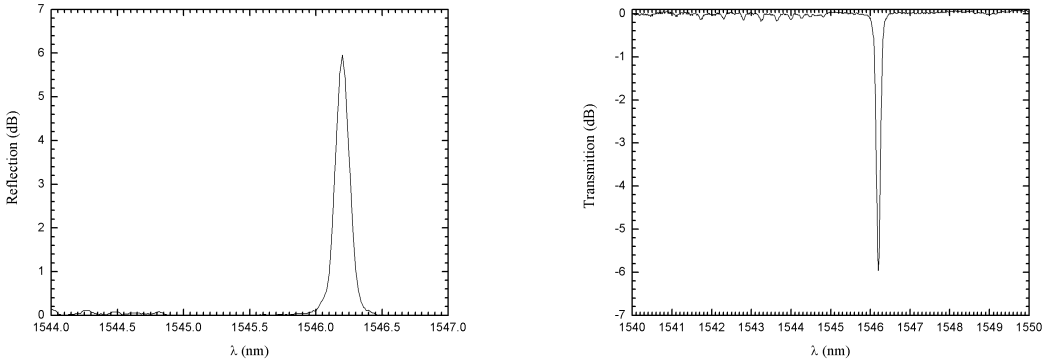

(a) Spectrum obtained in reflection.

(b) Spectrum obtained in transmission.

Figure 3.2: Results obtained in the analysis of a FBG centered in 1546.2 nm, in reflection and transmission [1].

Any external parameter can cause a perturbation on the period grating, thereby changing its performance, in particular the *Bragg* wavelength. In 1997, Kersey *et al.* [28], reviewed FBG sensors work, especially its performance under vibrational changes, pointing out that if $\delta\lambda$ is the range of wavelength where the reflective coefficient is higher, then,

$$\frac{\delta\lambda}{\lambda_B} = \frac{\delta n}{n_{eff}} \tag{3.2}$$

Reflections from each successive period will be in phase for a satisfied *Bragg* condition. For external perturbation of strain and temperature, typically the shift in the *Bragg* wavelength is given by:

$$\Delta\lambda_B = 2[\Lambda\frac{\delta n_{eff}}{\delta\varepsilon} + n_{eff}\frac{\delta\Lambda}{\delta\varepsilon}]\Delta\varepsilon + 2[\Lambda\frac{\delta n_{eff}}{\delta T} + n_{eff}\frac{\delta\Lambda}{\delta T}]\Delta T. \tag{3.3}$$

Commonly, the values for temperature and strain sensitivities are $12pm/^{o}C$ and $1.3pm/\mu\varepsilon$, respectively. Analyzing these physical parameters individually, it is possible to assess the type of behavior that it is expected. First, the response to temperature perturbations, which

results from the silica's expansion and from the refractive index temperature dependence, has an expected behavior of a linear relation between the wavelength shift, $\Delta\lambda$, and the temperature variation, ΔT.

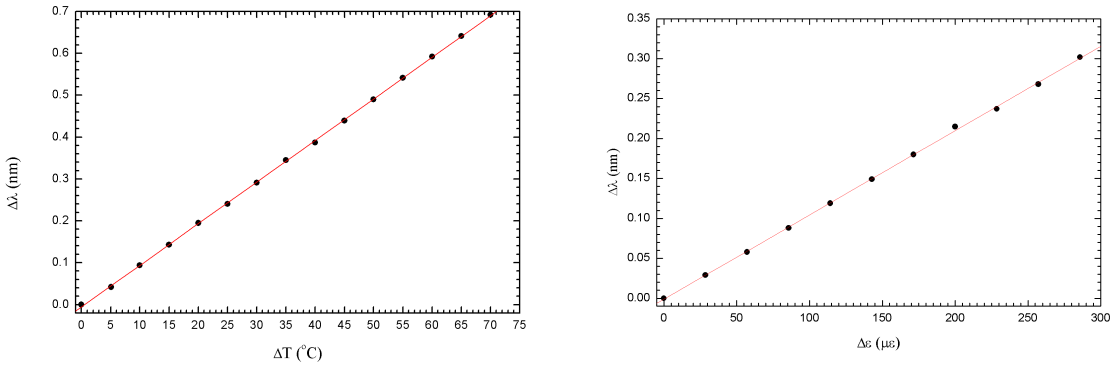

(a) Wavelength shift dependence on temperature.

(b) Wavelength shift dependence on strain.

Figure 3.3: Characterization of a FBG on temperature and strain.

This dependency can be written in order to thermal expansion (α) and thermal-optic (ξ) coefficients as,

$$\Delta\lambda_B = \lambda_B[\frac{1}{\Delta}\frac{\delta\Delta}{\delta T} + \frac{1}{n}\frac{\delta n}{\delta T}] = \lambda_B[\alpha + \xi]\Delta T. \tag{3.4}$$

By knowing that, and the thermal expansion and thermal-optic coefficients, it is possible to conclude which one controls the wavelength shift when the temperature is varying. Analyzing now the FBG expected response to strain, which is also a linear relation between the wavelength shift and the applied strain, as it can be seen in Figure 3.2(b) and, it comes from the refractive index variation due to the photo-elastic effect and also from the physical deformation of silica. This behavior can be summarized by the equation (3.5), where p_e is the photo-elastic coefficient [30].

$$\Delta\lambda_B = \lambda_B[\frac{1}{\Delta}\frac{\delta\Delta}{\delta\varepsilon} + \frac{1}{n}\frac{\delta n}{\delta\varepsilon}] = \lambda_B[1 - p_e]\Delta\varepsilon. \tag{3.5}$$

The expected behavior of the *Bragg* wavelength can be seen in Figure 3.3, where two gratings were tested in deformation. The test was performed by applying a deformation in one FBG, while the other remains still. As it can be seen, the *Bragg* wavelength follows the applied deformation. By using FBGs, there are two options to perform the analysis: by wavelength shift or optical power variation, which corresponds to analyze the spectrum on the typical wavelength and power range, respectively [31]. It is possible to execute the same study using intensity sensors, such as Fabry-Perot cavities or micro-spheres, placed

on the fiber tip. These sensors enable cost reduction over the signal processing systems together with a simpler setup, since it only needs a source and a detector to perform the analysis.

3.2 Brief Review of Sensing Applications

In this section, it will be presented a review of applications using optical sensors coupled with 3D printing technique. Among several examples, the fiber optic accelerometer and the fiber optic pressure sensor will be explored as good candidates to develop the housing through 3D printing technique, not only due to their relevance in the field, but also for the relevant applicability as biomedical sensors. Knowing the influence of external parameters in light properties, and the consequences on incident signal, it is possible to draw conclusions about the system under analysis. Also, knowing the behavior of the optical sensor, it can be calibrated according to the needed operation. Optical sensors and configurations were studied in order to develop new structures in different areas, for instance monitoring constructions in civil engineering or, in a totally different area, assess intracranial pressure during surgical procedures. Some of these functions were implemented by combining FOS with interferometry, or simply by applying the sensor to a specific setup. Thus, fiber optic sensors also proved to be an attractive technology for biomedical applications, due to its intrinsic physical characteristics, such as the immunity to electromagnetic interference, associated with the versatility in remote sensing [27]. The more common working principles for biomedical applications are based on modulation of: intensity, wavelength and phase.

3.2.1 Fiber Optic Accelerometer

An accelerometer is a device used to measure the acceleration or deceleration in a moving object [32]. The most common accelerometers are capacitive, piezoelectric and piezoresistive, but the advantages of using a fiber optic accelerometer make them an excellent alternative. Particularly, due to their high sensitivity, reduced weight (compared with the electrical components) and relatively high signal-to-noise ratio [33]. Wei Su *et al.* [34], in 1996, purposed a two dimensional fiber optic accelerometer based on a force transducer, built from an optical birefringent material. It was verified that the performance level of this element was comparable to the best electrical accelerometers, and that improved the design and calibration procedures. It is possible to build 2D and 3D accelerometers [35, 36]. But, in order to monitor movements and promote biomedical applications, such

as a limb monitoring, it is important to assemble a 3D optical fiber accelerometer, in order to provide a complete study. For an FBG sensor to function as an accelerometer, the configuration of the sensor's structure must be suitable to sense the acceleration variations and to result on the expected Bragg wavelength shift. Sometimes the sensor needs to be coupled to a mechanical load to improve sensitivity. The resulting shift is then calibrated and converted to acceleration (see Figure 3.5) [32, 37]. This configuration may be implemented

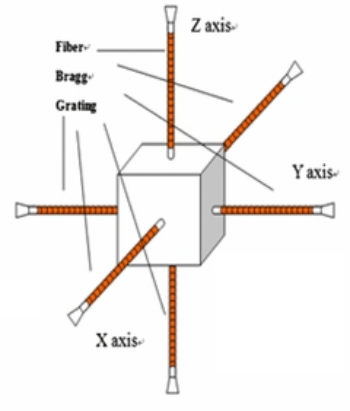

Figure 3.4: Diagram of a FBG accelerometer design.

in various biomedical sensors. For example, in monitoring patients who suffered a stroke in rehabilitation processes [38]. Rehabilitation is a dynamic process that allows patients to restore their normal function. Generally, patients experience difficulties in gait as a result of a stroke. In 2012, So *et al* [39], presented a cheap, convenient and efficient method to provide useful information about the treatment and its evolution, by gait analysis using wearable sensors. These sensors have to monitor the movement during the gait and, be able to conclude about the acceleration of the feet or legs. It can also be applied to an evaluation of progress in physical therapy, such as monitor the hand movement, each finger or wrist movement. Zhou *et al.* [40], in 2007, presented a review in human motion tracking for rehabilitation, it was presented a glove-based analysis with attached fiber optic sensors. In 2014, Fujiwara *et al.* [2], improved the previous idea, presenting a viable setup (see Figure 3.5), also using a glove that, through detection of angular displacements, could monitor finger movements.

3.2.2 Pressure Sensor

The three main fiber optic sensors used for pressure measurement are: intensity sensors, Fiber Bragg Gratings and Fabry-Perot. The FBG working principle was already discussed, it is based on changing the grating period; The principle behind intensity sensors is based

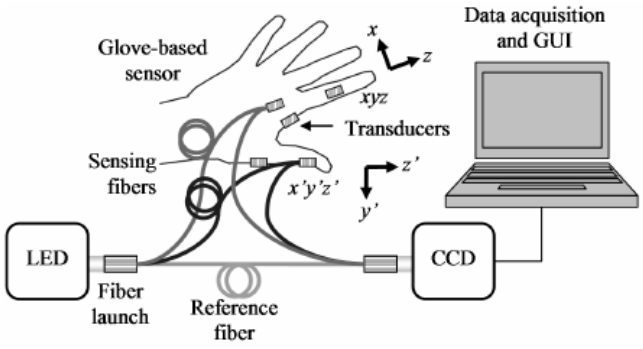

Figure 3.5: Proposed setup for sensing finger movements [2].

on the difference between a reflected beam from a deflecting diaphragm, that deflects with pressure, and the incident one; And, Fabry-Perot principle relies on the changing of the cavity length due to applied pressure [41].
Each one of these technologies has their own advantages and disadvantages, related to the cost of the equipment associated with or sensitivity issues.

Back in 2013, Roriz *et al.* [3], reviewed fiber optic pressure sensors for biomedical and biomechanical applications, and studied the evolution of biomedical pressure sensors, concluding that the greatest difficulty is the necessity of more *in vivo* tests, in order to present more turnkey solutions. Biomedical sensors for pressure measurements can evaluate in-

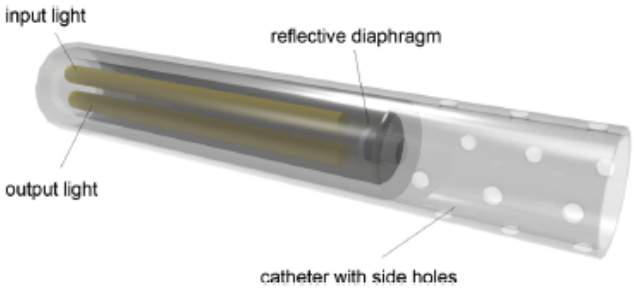

Figure 3.6: Example of a fiber optic pressure sensor, where is illustrated both optical fibers, for the incident and the reflected signal by the diaphragm [3].

travascular and intracardiac pressure, intramuscular or intracompartmental pressure, intra-articular pressure and intracranial pressure. Each sensor needs to be adapted, depending on how invasive is the technique. Similar to the described applications, there are others used not only in diagnosis, monitoring, and treatment, but also in minimally invasive surgery (MIS) where sensing catheters, smaller and accurate, are needed for monitoring the procedures [42, 43]. Again in biomedicine field, this kind of pressure sensor can be used to measure the heart rate, or to obtain the aortic pulse. The heart rate (HR) is the

rhythm or speed of the heartbeat, which is measured by the number of contractions of the heart (beat) per minute (bpm). The rate may vary according to the body needs, including the need to absorb oxygen and exhale carbon dioxide. The HR, generally, equals or is quite similar to pulse measured at any point on the body, where an artery is near the surface and is reachable to perform the measurement. However, to carry out precise measurements, the area of choice would be the neck, *Carotid Pulse*, or the wrist, *Radial Pulse*. Although, it is the carotid artery that features a more similar result to cardiac pulse due to its diameter, close to the diameter of the aorta.

In 2017, Yhuwana *et al.* [44], proposed a FOS for heart rate detection, successfully used to measure the amplitude and frequency of the heart rate signal, in a frequency range of 50-300bpm. This sensor could measure the HR with almost 100% linearity, according to the authors, which was an improvement from the proposed sensor in 1992, by Lindberg *et al.* [45], which in turn monitored respiratory and heart rate. Also, from the aortic pulse is possible to assess about lifetime, cardiac defects and mortality risk. In 2001, Safar *et al.* [46], related the aortic pulse wave velocity as an independent parameter to disclose a possible cardiovascular defect and, a potential risk patient, based on the relation between aortic pulse wave velocity and aortic stiffness, which is an index of heart problems.

The carotid pulse (neck region) can be examined by a health professional, with the patient supine and the trunk of the patient's body slightly elevated. During palpation, the examiner uses the receptors in the fingertips to sense movement of the arterial wall associated with the pressure pulse, as it passes by the site of palpation. This is a controversial method among the examiners, because it highly depends on the perception and preferences of the examiner. There are many opinions about how many and which fingers should be used to perform the analysis. Apart from these incompatibilities, it is still possible to confuse the own fingertip pulse with the one under analysis [46, 47].

In 2013, was developed a biomedical optical sensor that can register the carotid pulse using a certain structure (see Figure 3.8) and a FBG, by Cátia Leitão *et al.* [4].

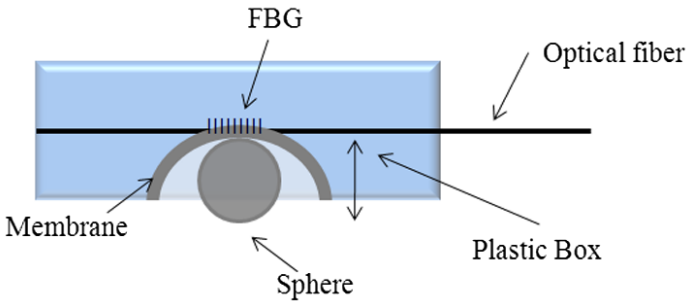

Figure 3.7: Schematics of the fiber Bragg probe configuration [4].

The developed sensor was characterized and calibrated. And, by using a PZT with a

movement range close to the aortic movements (see Figure 3.9), it was possible to register the Bragg grating response, which is similar to the expected from the carotid movements.

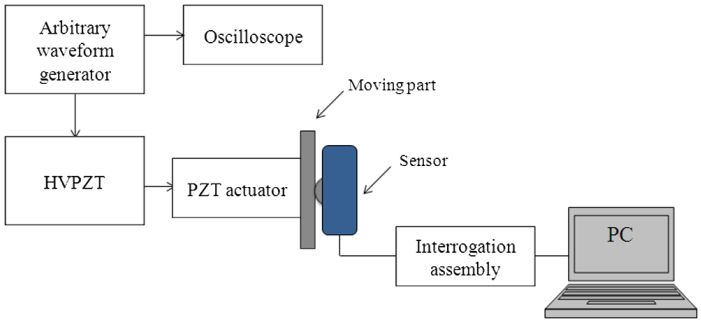

Figure 3.8: The setup used to preform the mechanical characterization with arbitrary waveforms [4].

Considering all the described disadvantages and the developed FOS, it is proposed the development of a reliable and accurate FOS that could intend pressure analysis, implementing the 3D printing technique for the FOS housing, allowing among others, the biomedical application.

Chapter 4

Optical Fiber Pressure Sensor

Optical fiber sensors, especially FBG, have been used in pressure measurements because of its characteristic high sensitivity and well known behavior. The typical range of measurement is from $0MPa$ to $0.5MPa$ and, the determined sensitivity between this range is of the order of $-1.0 \times 10^{-3} nm/MPa$ [48, 49].

Also, FOS embedded in a polymer material have also been used due to the resistance that the sensor acquires and, consequently, to its protection and adaptability in harsh environments [50, 51].

The 3D printed optics combine optic elements with the 3D printing technique, not only by innovating the fabrication of ophthalmic lenses, but also by allowing to embed the optical sensor in a 3D printed structure [14]. This new procedure puts together these two areas of expertise, allowing to explore the main advantages of each one.

In this chapter, an optical fiber pressure sensor, based on a fiber Bragg grating embedded in a 3D printed structure, is presented. The working principle is based on the change on the grating period, due to the applied pressure, as explored in chapter 3.2.2.

4.1 Simulation and Experimental Configuration

The fabricated sensor consists of a circular base that supports the sensor head itself. That is based on a three cantilever structure connected with a central mass, in order to promote the strain of the grating with applied pressure (see figure 4.1). The object was designed and dimensioned in a proper software, suitable and commonly used for 3D printing, Solidworks. The FBG positioning in the cantilever was studied through the same software used for the

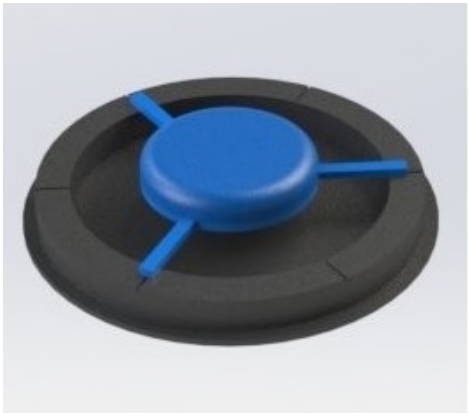

Figure 4.1: Pressure sensor designed: sensor's base (black) and head (blue).

sensor's dimensioning. It was possible to simulate the structure behavior under applied pressure and, assess two important facts: first, by using a three cantilever structure the applied pressure is uniform in all the structures, so the sensor's response will be the same regardless of the cantilever where is embed; second, that the most sensitive area is on the cantilever just before the junction with the central mass (see Appendix B).

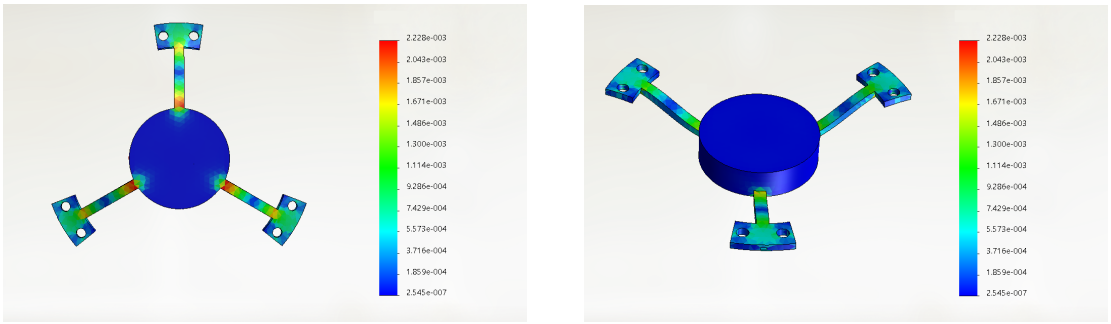

(a) Strain simulation bottom view.

(b) Strain simulation lateral view.

Figure 4.2: Strain simulation to assess the behavior of the sensor head under applied pressure, approximately $5kPa$.

The 3D printing process can influence or change the response of the sensor, due to the stresses and tensions associated with the process temperature and material's accommodation. Even when this anomaly is presented in the sensor's spectrum, the sensitivity of the FBG it isn't affected. As long as the behavior of the FBG is known, before and after the printing process, the sensor can be calibrated and the defect corrected.

Two different analysis were performed, an optical and electric analysis. Performing the first one, it was possible to observe how the *Bragg* wavelength reacted to the applied pressure and, study the hysteresis of the material, assessing its response precision. And, from the

electric analysis, it was possible to observe how the FBG reacted to vibration. The main setup used to perform these tests is the following. The interrogation system was adjusted for each analysis, an OSA was used for the optical analysis, while for the electrical one, the OSA was replaced by an oscilloscope associated with a photodiode.

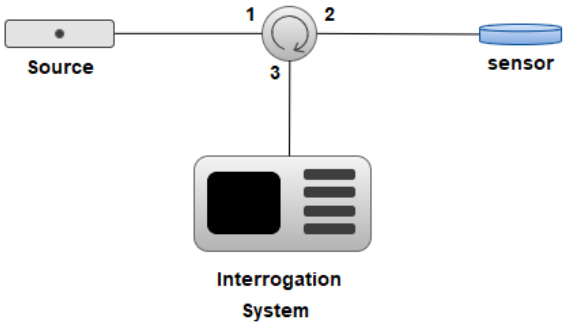

Figure 4.3: Main setup for both analysis.

In order to test the fabricated sensor at low frequencies, was used a mechanical vibration system, to apply pressure on the sensor's head, together with the previous setup. The mechanical system, consisting of a piston and a base, is connected to a signal generator, with the purpose of moving the piston in a selected frequency. These equipments allow the reproduction of low frequencies, similar to those reproduced by the heart rate, which can be an interesting biomedical application.

4.2 Experimental Results

The fabricated pressure sensor is depicted in Figure 4.4. The sensor's base has a cylindrical form with $59mm$ of external diameter, $45mm$ of internal diameter and 5mm of height. And, the sensor's head has three cantilevers with $12.50mm$ of length and a central mass, with a diameter of $20mm$ and $5.20mm$ of height. This three cantilever configuration was studied, as presented in chapter 4.1, and it was considered the ideal one, due to the sensitivity it presented to strain.
The sensor was fabricated using an helloBEEprusa 3D printer with a vertical resolution of $200\mu m$. In this work, the 3D printed technique is used to embed the sensor in the respective 3D printed polymer. All the sensors were embedded in PLA (polylactic acid), which is a thermo-polymer filament, and the printing technique used to embed all the fabricated sensors was the extrusion deposition method.
The printing process begins after uploading the STL file, with information of the designed

object. The procedure is paused and the FBG is fixed. After placement of the sensor, the procedure is resumed and finished. Finally, it is obtain a 3D printed object with an embedded and functional FBG.

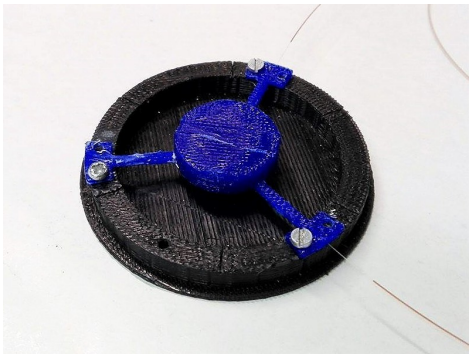

Figure 4.4: Fabricated optical fiber pressure sensor prototype.

The grating embedded has a characteristic and expected *Bragg* wavelength, as explored in chapter 3.1 (figure 3.2.a), centered at $1544.171nm$ before the printing process, and a length of $2.5mm$. After the 3D printing process, it can be observed that the central wavelength suffers a small shift, to $1543.069nm$, due to the grating contraction. And, a defect in the spectrum appears as a second wavelength peak. This defect or deformation is due to a non

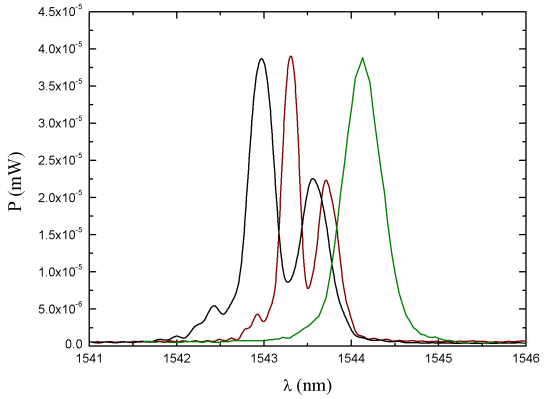

Figure 4.5: Reflection spectrum of the sensor, before (black) and after (green) the printing process with none applied pressure and, after the printing process with applied pressure (red).

uniform contraction in the grating. The printing process, particularly the fact that the polymer is partially melted and only after solidifies into the desired shape, promotes stresses in the embedded sensor. Those stresses affect the FBG and cause these spectrum deformations.

4.2.1 Pressure Characterization

The pressure characterization was performed using loads with different masses, and the tests were performed with different load steps: $250g$, $100g$ and $50g$. Several analyses were made, first, to assess the material hysteresis, the sensor was loaded until different values for each step. With the $250g$ load, four measures were registered, but it was possible to verify that the sensor is very sensitive to the load in question, especially when it comes to its geometry, the cantilevers could break or be deformed. So, the load step was reduced. The material hysteresis was again tested for $100g$ and $50g$ steps. With the $100g$ steps, the sensor was loaded until the $600g$ and then unloaded, always registering the shift of central wavelength in seven repetitions. The same procedure was adopted for the $50g$ steps. The sensor was also loaded and unloaded until $300g$ in seven repetitions and, the central wavelength's shift was registered.
The applied pressure is given by:

$$P = \frac{F}{A} \tag{4.1}$$

where,

$$F = mg \tag{4.2}$$

Knowing the applied load and surface area, it was possible to determine the applied pressure and evaluate the *Bragg* wavelength shift and, consequently, the material hysteresis.

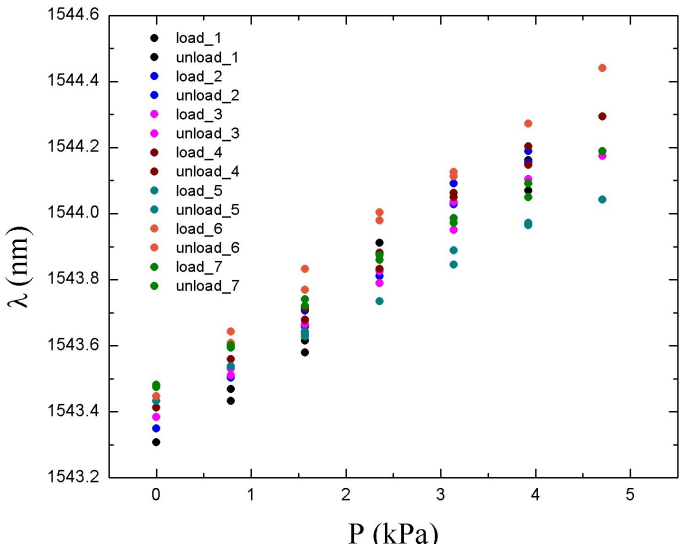

Figure 4.6: *Bragg* wavelength values of seven consecutive loads and unloads for $100g$ steps.

The results for load and unload with 50g steps are equal to the ones presented in Figure 4.6, and its pressure range is from $0kPa$ to $2.5kPa$, which fits in the pressure range presented in Figure 4.6. Likewise, through the seven consecutive tests, the *Bragg* wavelength mean value was calculated, for 100g and 50g load steps, and the *Bragg* wavelength shift was determined as a function of pressure (Figure 4.7), as well as the corresponding sensitivity, $178 \pm 3.64pm/kPa$.

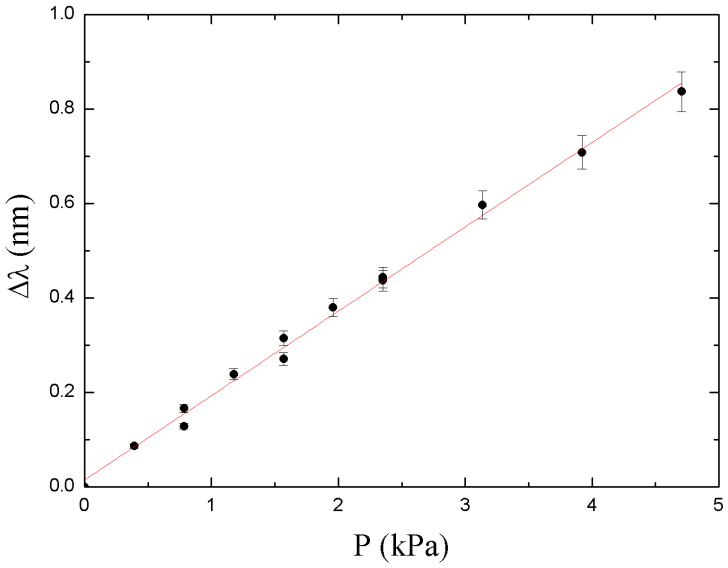

Figure 4.7: *Bragg* wavelength shift of *Bragg* wavelength mean values as a function of pressure.

In order to fully characterize the sensor, the resolution and measurement error were determined. For these calculations the $100g$ load was used. For the resolution calculation, twenty consecutive measurements were performed, ten with $0g$ load and another ten with $100g$ load. The result consists of two distinct levels, that correspond to two wavelength values, $1543.60nm$ and $1543.87nm$.
By analyzing it and through the wavelength variation between the levels, it was possible to determine the minimum value detected by the sensor, a value of $11.85g$, which corresponds to $0.092kPa$. To assess the measurement error, the *Bragg* wavelength was registered using a 100g load. The result was a wavelength shift of $0.0024nm$ and a sensitivity of $-6.5 \times 10^{-9} \pm 4.0 \times 10^{-9} pm/s$, also represented on figure 4.8, second level.

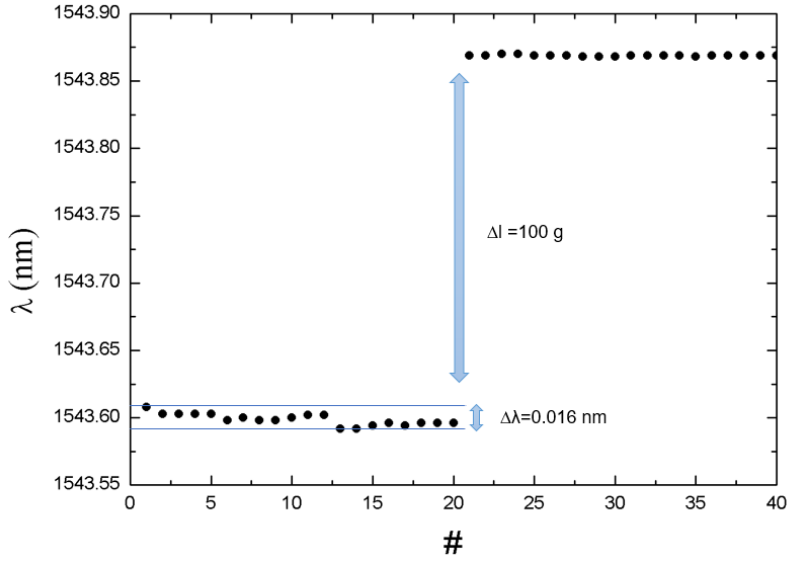

Figure 4.8: *Bragg* wavelength variation for twenty consecutive measures of $0g$ and $100g$ loads.

One more analysis was performed, in order to assess the offset time of the assembled sensor, this is the time that sensor needs to adjust to applied load and have a constant measurement. The test was conclusive and it was verified that the sensor delay is $1.5s$.

4.2.2 Vibration Characterization

This characterization was helpful to prove the concept of low frequencies detection and, reproduction of the transmitted signal by the fabricated sensor. Two setups were tested as explored in chapter 4.1. An optical analysis was performed, where the sensor response was displayed in optical power; and, an electrical analysis, where the sensor response was displayed in amplitude.

Focusing on low frequencies, the signal generator tuned to $5Hz$, $2.5Hz$ and $1.5Hz$. And, for each selected frequency the optical an electric signal were registered and analyzed accordingly. There was no filter implemented on the setup.

Despite some electrical noise, inherent in electric analysis, the obtained results were the expected ones. The previously selected frequencies were clearly displayed, proving the concept that fabricated sensor was sensitive to low frequencies and, that it can reproduce the transmitted signal only through direct contact.

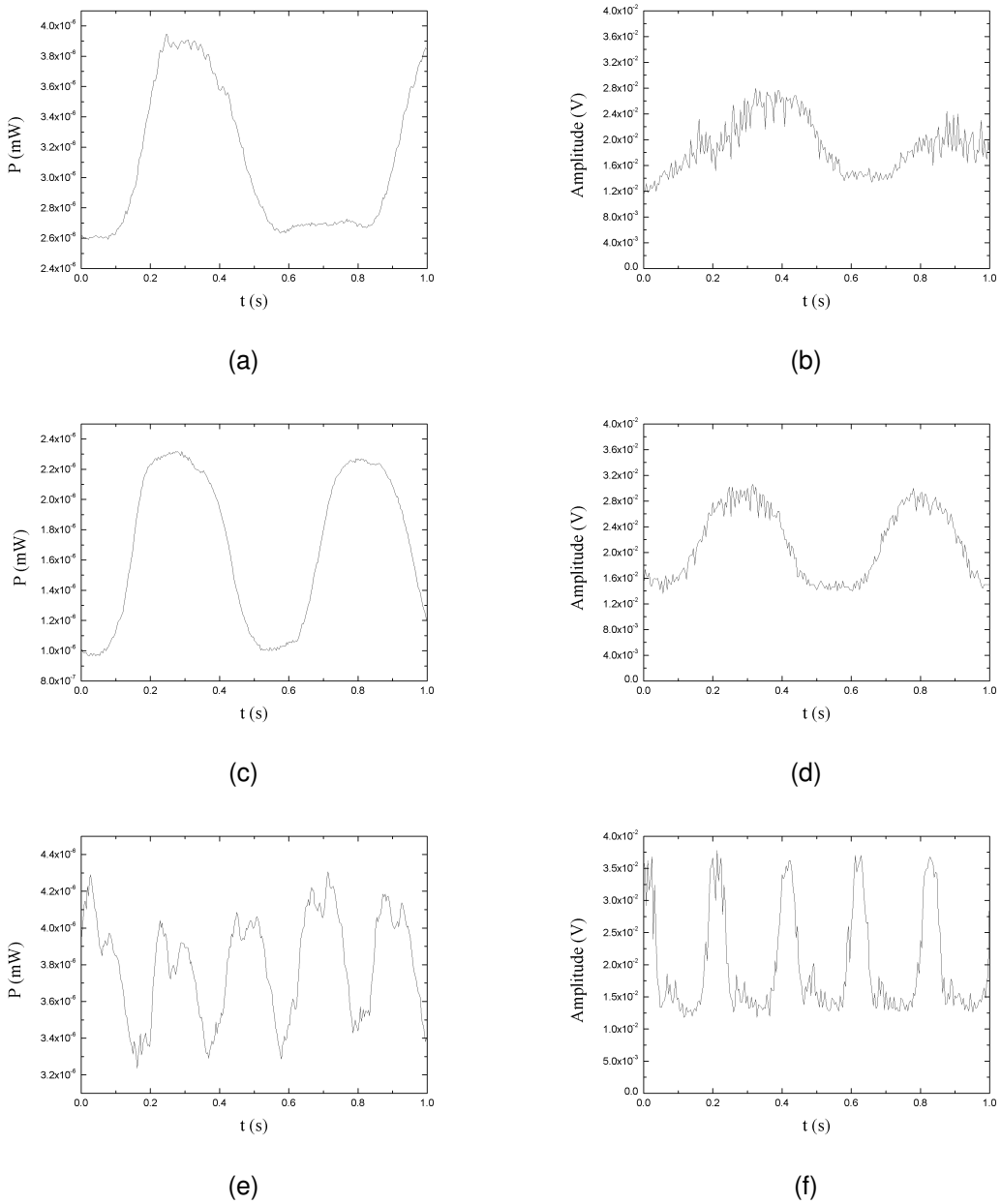

Figure 4.9: Reflection spectra for optic(left) and electric(right) analysis of the selected frequencies: $1.5Hz$, $2Hz$ and $5Hz$, respectively up bottom, left right.

Although the results were as expected, a signal processing was carried out to validate the same. Fast Fourier Transforms were calculated and, this analysis also confirmed the results obtained first, as can be seen in the figure 4.10.

During the testing, the sensor geometry was not affected, and the FBG embedded in polymer remained intact. The more likely point break is the interface between the polymer material and not embedded fiber, especially, if the fiber cladding is not embedded too.

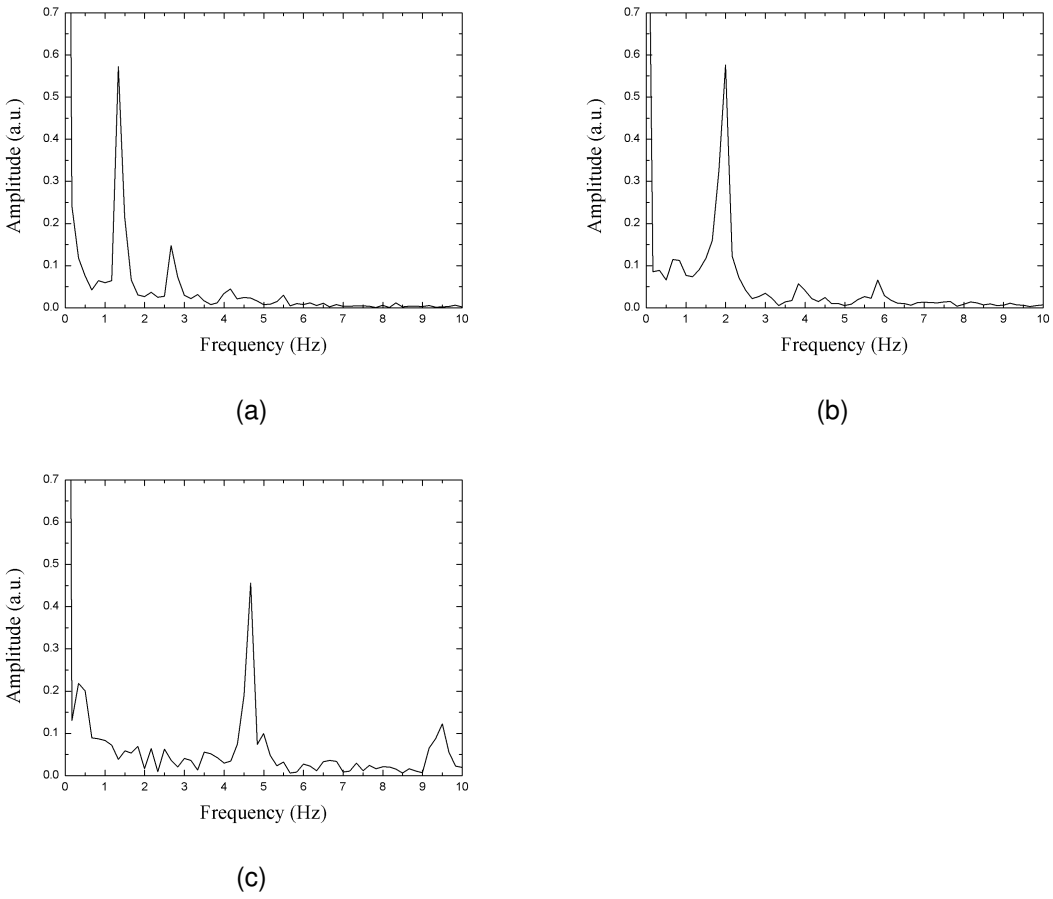

Figure 4.10: FFT representation of the signal reproduced by the assembled sensor, (a)$1.5Hz$, (b)$2Hz$ and (c)$5Hz$.

4.3 Discussions

The pressure sensing of the loaded 3D printed sensor was achieved for distinct loads. For pressure sensing, a sensitivity of $178 \pm 3.64 pm/kPa$ was obtained, for $100g$ steps and $50g$ steps, in a pressure range from $0kPa$ to $5kPa$. These results were obtained with a resolution of $11.85g$. The measurement error associated to all the performed tests was also determined in a value of $0.0024nm$ with a sensitivity of $-6.5 \times 10^{-9} \pm 4.0 \times 10^{-9} pm/s$. Also, it was possible to assess that the assembled pressure sensor has a time delay of $1.5sec$.

The vibration sensing was also achieved for different selected frequencies: $5Hz$, $2Hz$ and $1.5Hz$, simply using direct contact between the mechanical system and the sensor's head. The results obtained in both the performed analysis (optical and electrical) were coherent with expected, reproducing the frequencies of transmitted signal, as was confirmed by the calculation of respective Fourier Transforms.

Biomedical applications are a reliable option for the developed pressure sensor, as explored in chapter 3.2.2, this sensor can be used as a heart rate sensor. Comparing it with previously published results and different geometries, the developed sensor directly competes with the published results for vibration sensing [4] and, the technique to assemble the FBG housing, in addition of being innovative and a low-cost technique, also allowed similar results [50].

The sensor resisted all the tests and, its polymeric housing worked well, protecting the embedded optical sensor without compromising its reading. At the same time, the printed housing allowed the deformation of FBG in response to the applied pressure, which suggests a good response to diverse deformations, as it was proved with vibration characterization.

Chapter 5

Optical Fiber Accelerometer

An accelerometer is a device that measures the acceleration of a body in its own coordinates system, with the respective body at rest [52]. Traditionally, as explored in chapter 3.2.1, common accelerometers are piezoelectric, piezoresistive or capacitive based sensors [32]. Fiber optic accelerometers present a performance that matches and/or exceeds the previous sensors.

Acceleration measurements, monitoring structures (especially the identification of structural damage) or vibration measurements of electrical machines are some of the possible applications of optical fiber accelerometers. Particularly, considering the optical fiber advantages such as its flexibility and light weight, immunity to EMI and the possibility of remote sensing, among several others [53]. Certain optical sensors and different configurations were tested, depending on the desired application [54, 55]. Typically, these designs are tested in a frequency range of [0,200] Hz and achieved an acceleration maximum value of 25G [37, 32]. However, and despite the typical results, the ideal sensor must be practical, effective and low-cost. Ideally, the sensor must be optimized according to the application for which it was designed, so that its properties can meet the necessary requirements for the desired application.

In this chapter, an optical fiber accelerometer is presented, based on FBG sensors embedded in 3D printed polymer, for acceleration measurements. Three structures were assembled, 1D, 2D and 3D configurations, in a previously studied and optimized cantilever structure. A vibration and displacement characterization were performed in all the assembled configurations.

5.1 Simulation and Experimental Configuration

The fabricated main structure consists on a cubic structure and the optical sensors are embedded in a cantilever configuration placed on its faces (see Figure 5.1). This configuration was adopted aiming a possible biomedical application for monitoring movements, mainly the wrist movement. Implementing this kind of sensor in an hospital environment, would enable the monitoring of treatments and support diagnosis, for instance rehabilitation treatments, thereby improving the patient follow-up.
In order to assemble this kind of sensor, it was designed a structure that could be easily handle by a human hand, a cubic structure with $50 \times 50 \times 50mm$ dimensions.

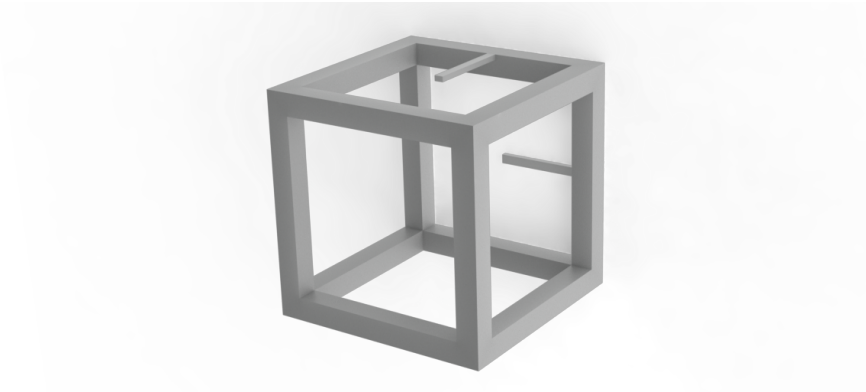

Figure 5.1: Fiber optic accelerometer simulation and design: a cubic structure with a cantilever configuration placed.

To promote the optimization of the sensor, the 3D printing technique was introduced. By using this technique is possible to adapt the sensor's structure to the desired application. The sensor was designed and fabricated using the same technique that was explored back in chapter 4 section 4.2, was designed through Solidworks software and, printed by an helloBEEprusa 3D printer.
As noted above, the printing technique influences the *Bragg* wavelength, but once the behavior of the sensor was known before printing, the procedure to cancel this defect is the same and, is based on the calibration of the sensor after printing. Several simulations were performed, in order to assess the best configuration to print and where to place the FBG, so that it could be placed on structure's most sensitive point, allowing the maximum deformation on the *Bragg* period with the acceleration variation (see Appendix B). Pursuing this, different formats were studied by varying the physical parameters of the structure and, taking into account the cantilever configuration, two formats were selected and are displayed in figure 5.2.

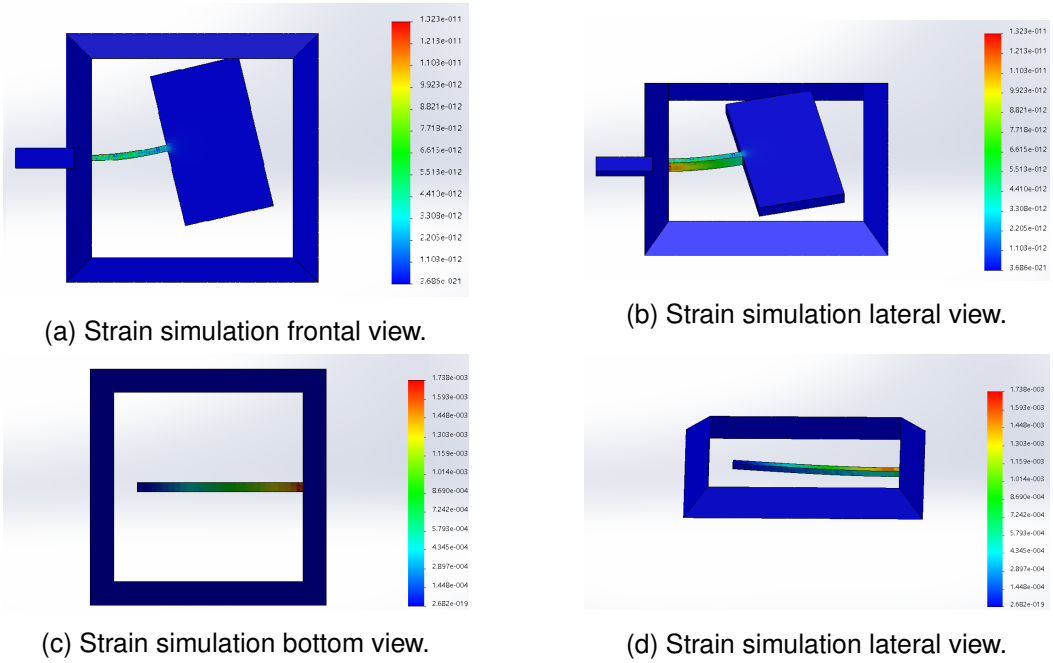

(a) Strain simulation frontal view.

(b) Strain simulation lateral view.

(c) Strain simulation bottom view.

(d) Strain simulation lateral view.

Figure 5.2: Strain simulation to assess the most sensitive spot under applied force.

The selected dimensioning produced the best results under applied strain and, the most sensitive point was discovered, as expected, to be the area immediately after the junction between cantilever and squared structure. In general, for the three configurations, 1D, 2D and 3D, a displacement and vibration characterization were executed. The configuration shown in image 5.2 (a) and 5.2 (b) was fabricated and tested in a 3D configuration while, the structure displayed on figure 5.2 (c) e (d) was tested in 1D and 2D configuration. The experimental setup adopted to execute the optical fiber accelerometer characterization is based on an OSA, as the interrogation system; an optical circulator, to promote a one-way circulation and, a broadband source with a $100nm$ range, $[520, 620]nm$. Implementing the described experimental configuration, it was possible to perform an optical analysis and assess how the sensor responds to applied displacement. For that, a displacement of $1mm$, with steps of $0.1mm$, was applied to the sensing part of the accelerometer (cantilever structure) and, the relation between *Bragg* wavelength shift and applied displacement was obtained. Through this relation, the sensor's sensitivity and precision can be determined, thus enabling a vibrational study. The referred study consists on ascertain the position, velocity and acceleration characteristic of the sensor when vibration is applied.

To prove the concept of monitoring movements, based on the sensing of acceleration variation, an electrical analysis was executed. For that, an oscilloscope associated with a photodiode was used as interrogation system, along with a tunable laser source, tuned to the most sensitive wavelength, according with each FBG and its characteristic spectrum.

5.2 Experimental Results

This section is divided into three parts, each one describes and presents the obtained results for the 1D, 2D and 3D optical fiber accelerometer configuration.
Clearly, after obtaining the 1D configuration, the remaining two are obtained by adding another face at the cubic structure, with an embedded sensor. Nonetheless, for the monitoring of cognitive movements a 3D configuration is needed and, by performing an electrical analysis and a proper characterization, it was possible to prove the concept.
The printing method adopted was also based on the embedding of optical sensor in the printed polymer (PLA), by pausing the process, placing the *FBG* and resume it once more. The *FBGs* were measured in reflection and, had two different lengths, $1mm$ and $2.5mm$, with a centered wavelength of $1550nm$.

5.2.1 1D Configuration Characterization

For the 1D optical fiber accelerometer characterization, a cubic structure with $50 \times 50 \times 50mm$ dimensions was fabricated, where only one optical sensor was embedded, and it is displayed in Figure 5.3. The cantilever structure has a thickness of $1.2mm$ and $20mm$ in length.

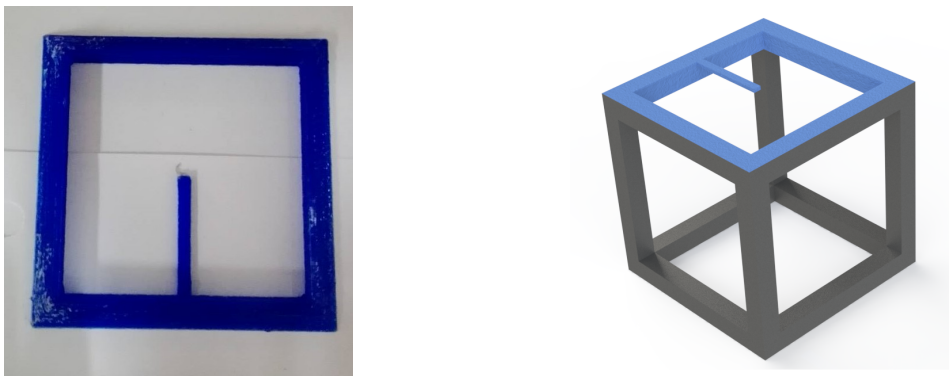

(a) (b)

Figure 5.3: (a) 3D printed part for the 1D optical fiber accelerometer and (b) its simulation.

The sensor's characterization began with displacement characterization. It was applied a displacement of $1.0mm$, with $0.1mm$ steps, to the cantilever's edge, using a translation stage. Meanwhile, the *Bragg* wavelength shift was registered and displayed in function of displacement, as well as the variation of optical power.

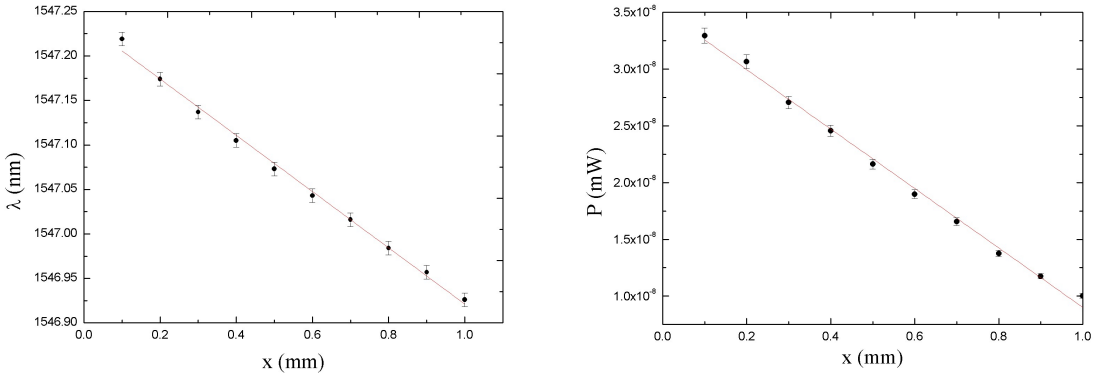

(a) *Bragg* wavelength variation. (b) Optical power variation.

Figure 5.4: Results of displacement characterization.

By evaluating this characterization, it was possible to assess the sensor's sensitivity to displacement in function of *Bragg* wavelength shift and optical power. As optical power and wavelength shift are directly proportional to displacement, a linear fit was determined. From this fit, sensitivities of $-316 \pm 7.20 pm/mm$ and $-2.6 \times 10^{-8} \pm 6.2 \times 10^{-10} mW/mm$ were obtained, respectively. The optical power analysis was executed by fixing the most sensitive wavelength, in this case $1547.710nm$.
The vibration characterization was implemented by applying vibration to the cantilever. From optical power analysis in function of applied displacement, it was possible to determine the position, velocity and acceleration produced by the applied vibration.

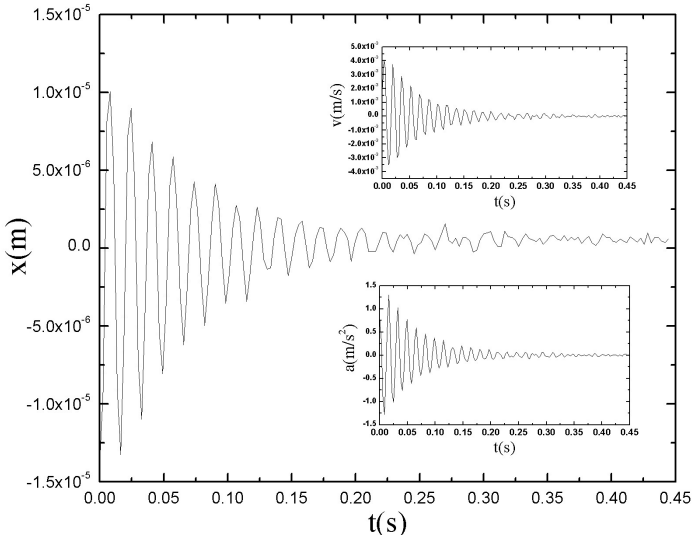

Figure 5.5: Vibration characterization: Position, velocity and acceleration determined.

Considering the previous results, the period and oscillation frequency were estimated, in $0.0167sec$ and, approximately $60Hz$. Also, by analyzing the acceleration signal, it was calculated a maximum of $0.15G$.

Likewise, an electrical analysis was performed to test the ability of the sensor on sensing acceleration variation. For that, the cubic structure was assembled, as the one presented in figure 5.3(b) and, a tunable laser was used, tuned to the most sensitive wavelength, $1546.7nm$. After setting a reference axis, corresponding to zero amplitude, the sensor was moved, replicating the wrist movement, and it was possible to register a variation in the signal's amplitude (V) in function of time (s). The change in amplitude is due to the sensor's response to acceleration in different positions along the cantilever configuration, which promotes a high sensitivity when it undergoes deformation.

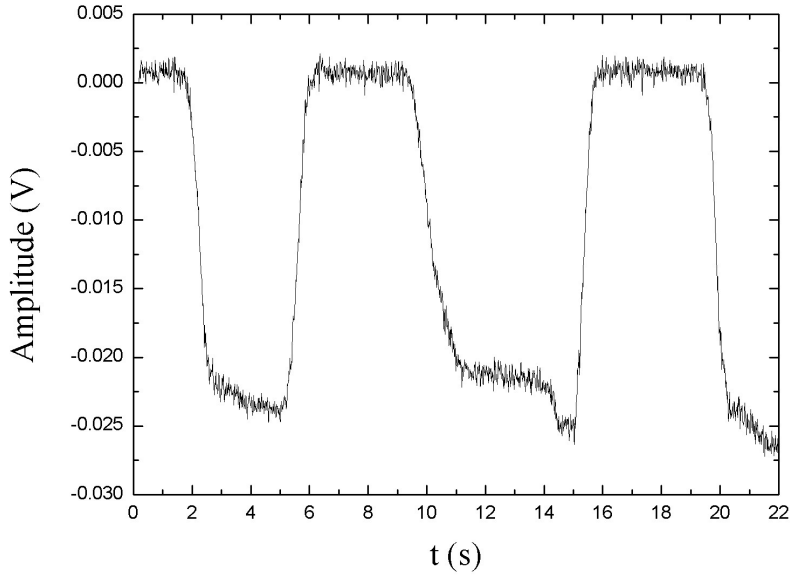

Figure 5.6: Variation of amplitude as a function of time.

5.2.2 2D Configuration Characterization

Although, the 2D optical fiber accelerometer characterization could be performed by simply adding another part, equal to the one presented in the previous section, another two parts were printed with different dimensions. This change in part sizing consists in increasing the length of cantilever structure, which improves the sensor's response and its sensitivity. The dimensions of the cubic structure remain the same, while the cantilever has the same thickness, but $35mm$ in length.

Two structures, as represented in Figure 5.7.(a), were printed and characterized in displace-

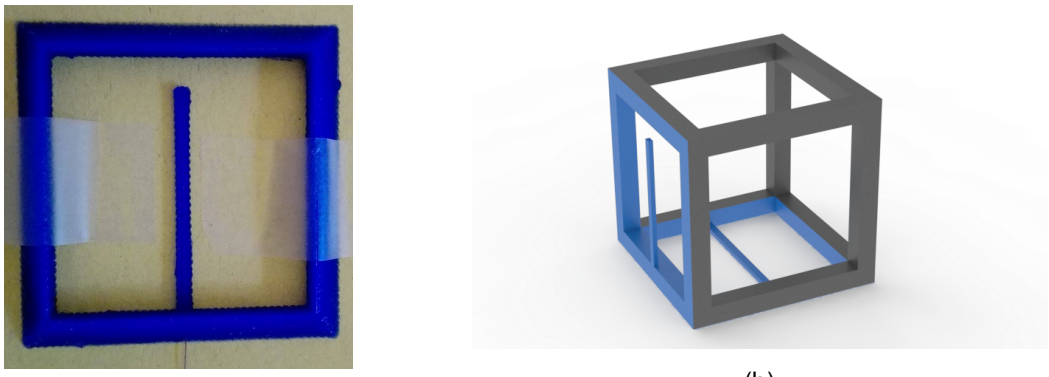

(a) (b)

Figure 5.7: (a) one 3D printed part for 2D optical fiber accelerometer and (b) its simulation.

ment and vibration. As explored back in section 5.2.1, the displacement characterization was performed by applying a displacement of $1.0mm$, with $0.1mm$ steps, employing the same procedure. The sensor's behavior was registered and the relation between *Bragg* wavelength and optical power in function of displacement was displayed. These relations are both directly proportional and so, a linear fit was determined. The optical power analysis was executed by fixing the most sensitive wavelength, in this case $1547.727nm$, and noting the corresponding power values as a function of the displacement. For the first sensor, the referred relations are displayed in figure 5.8., and sensitivities of $459.8 \pm 12.82pm/mm$ and $-4.3 \times 10^{-5} \pm 2.7 \times 10^{-6} mW/mm$ were achieved, respectively, for *Bragg* wavelength and optical power in function of displacement.

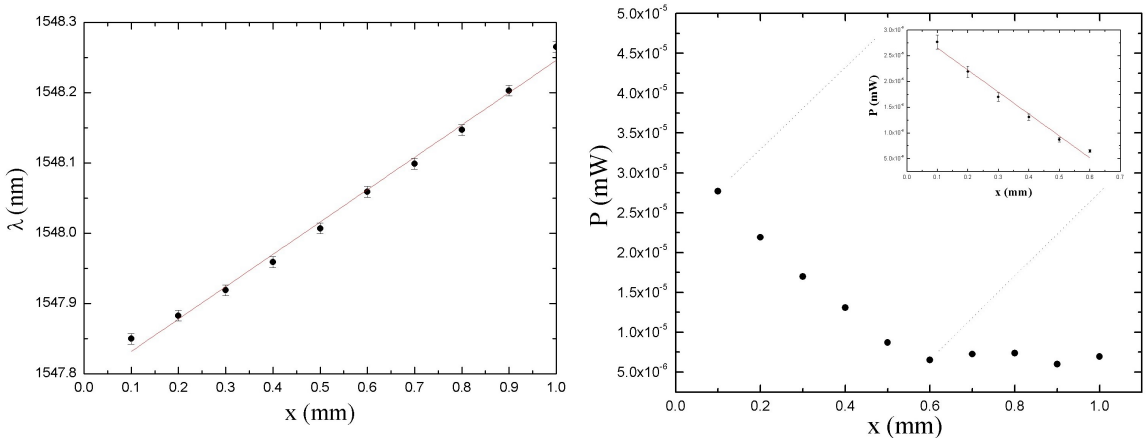

(a) (b)

Figure 5.8: Results of displacement characterization for the first printed sensor: (a) *Bragg* wavelength and (b) optical power behavior.

As it is possible to observe in figure 5.8.(b), the relation between optical power and displacement it is not linear starting at $0.6mm$. This fact is due to the great sensitivity achieved for *Bragg* wavelength. The shift of the characteristic spectrum is so meaningful, due to displacement, that the most sensitive wavelength is changed during measurement, which influences the optical power behavior and therefore its analysis.
For the second sensor an equal characterization was performed and similar behaviors were obtained for the same studied parameters. Sensitivities of $13.5 \pm 0.51pm/mm$ and $3.65 \times 10^{-6} \pm 9.89 \times 10^{-8}mW/mm$ were achieved, respectively, for *Bragg* wavelength and optical power in function of displacement. The determined sensitivities are inferior than the ones obtained from the first sensor. This fact is directly connected with the *FBG* positioning during the printing process.

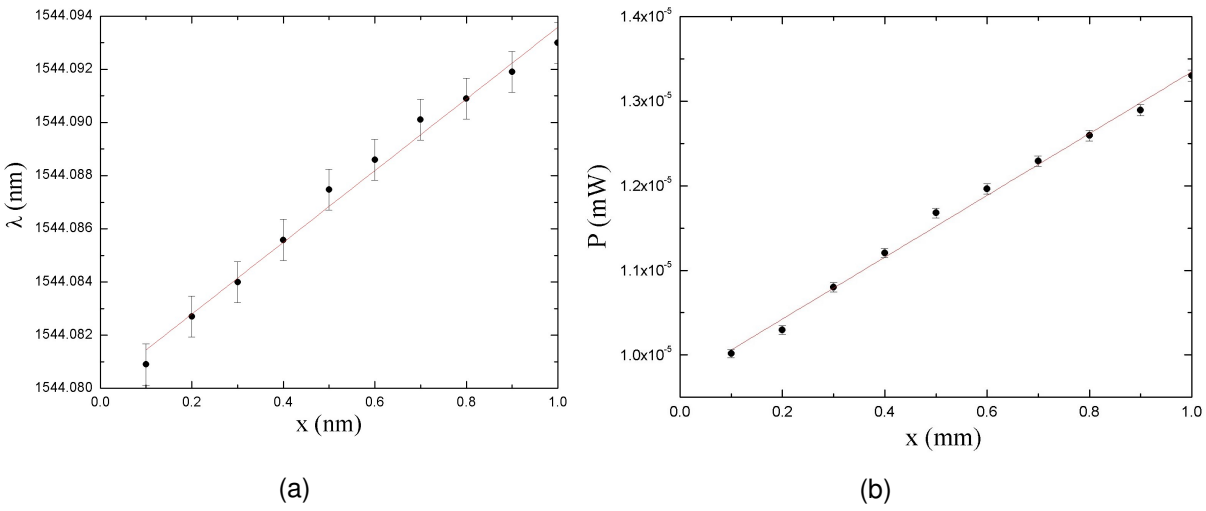

Figure 5.9: Results of displacement characterization for the second printed sensor: (a) *Bragg* wavelength and (b) optical power behavior.

The procedure to perform the vibration characterization was similar to the one used in the 1D optical fiber accelerometer. The position, velocity and acceleration produced by the applied vibration were determined, through the results of optical power analysis, for both sensors. The period and oscillation frequency were also possible to estimate and the results are coherent with the expected, $0.009sec$ period and $111Hz$, approximately for both printed sensors. The acceleration result had a calculated maximum of $1.5G$ for the first sensor and, $5G$ for the second sensor.

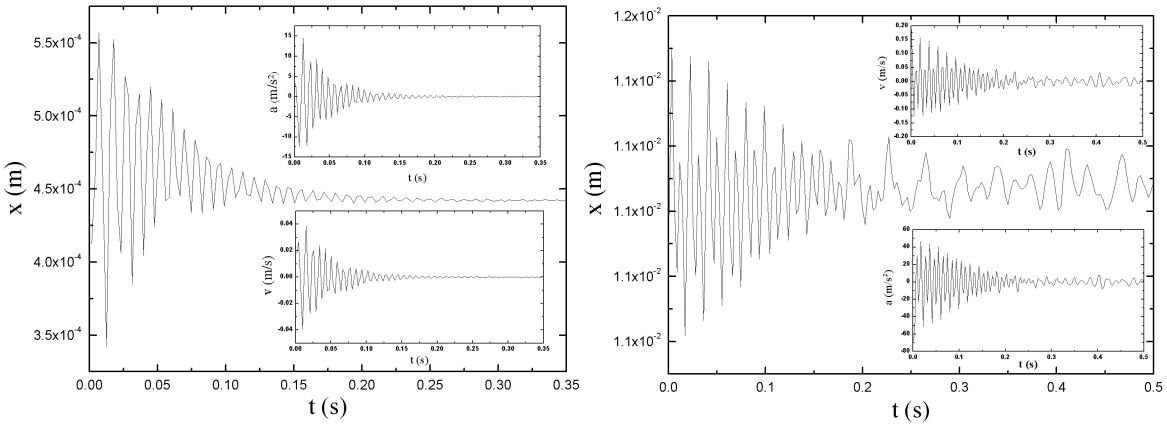

Figure 5.10: Results of vibration characterization for both printed sensors: (a) first and (b) second sensor.

In order to prove the concept of acceleration variation sensing an electric analysis was executed. The cubic final structure was assembled containing both characterized sensors. Also, two tunable lasers and two photodiodes were used, with the lasers tuned to the most sensitive wavelengths. The accelerometer was moved, again replicating the wrist movement and, after setting a reference axis and a proper signal processing, it was possible to observe a variation in the signal's amplitude.

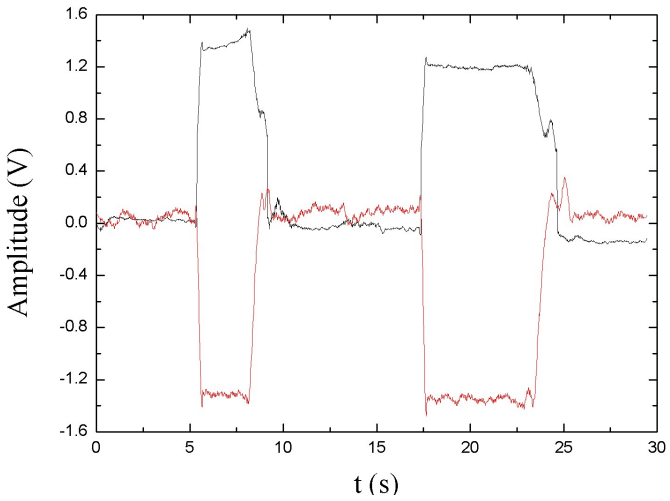

Figure 5.11: Variation of amplitude as a function of time.

5.2.3 3D Configuration Characterization

To fabricate the 3D optical fiber accelerometer the dimensions and geometry of the printed parts, that embed the FBGs, were adapted. A different cantilever geometry was designed, with a mass on the edge, to improve the vibration sensing. Thus, the length of the cantilever was reduced to $15mm$ and, a rectangular mass, of $17.5mm$ wide and $30mm$ length, was introduced.

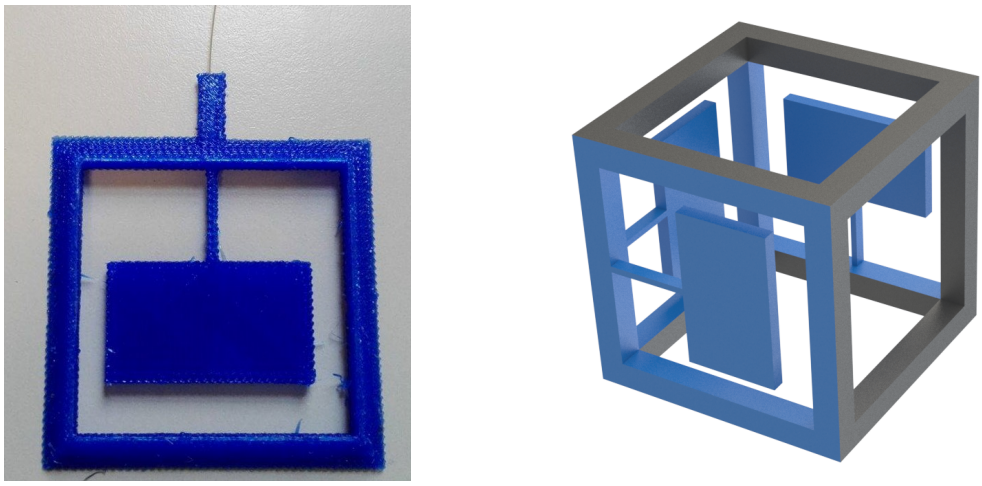

(a) (b)

Figure 5.12: 3D optical fiber accelerometer: (a) one of the printed parts and (b) its simulation.

Three equal parts, as displayed in figure 5.12(a), were printed through the same printing method and with the same printing material as referred to before. All three parts were characterized in displacement and vibration and, finally, the cubic structure was assembled (as displayed in figure 5.12(b)) and the vibration sensing was tested in three directions.
First, the displacement characterization was carried out by applying a displacement of $1.0mm$, in $0.1mm$ steps, on the cantilever's edge mass. As the displacement was applied, the *Bragg* wavelength shift was registered and, the result was the expected, a linear relation between the two parameters. From this analysis and by fixing the most sensitive wavelength, it was possible to evaluate the relation between optical power and displacement. The result was also the expected, a linear relation and, as such a linear fit was determined. This was the procedure followed for the displacement characterization of the three printed sensors. From the determined fit, the sensitivities of *Bragg* wavelength and optical power to applied displacement were determined and, are presented on table 5.1.

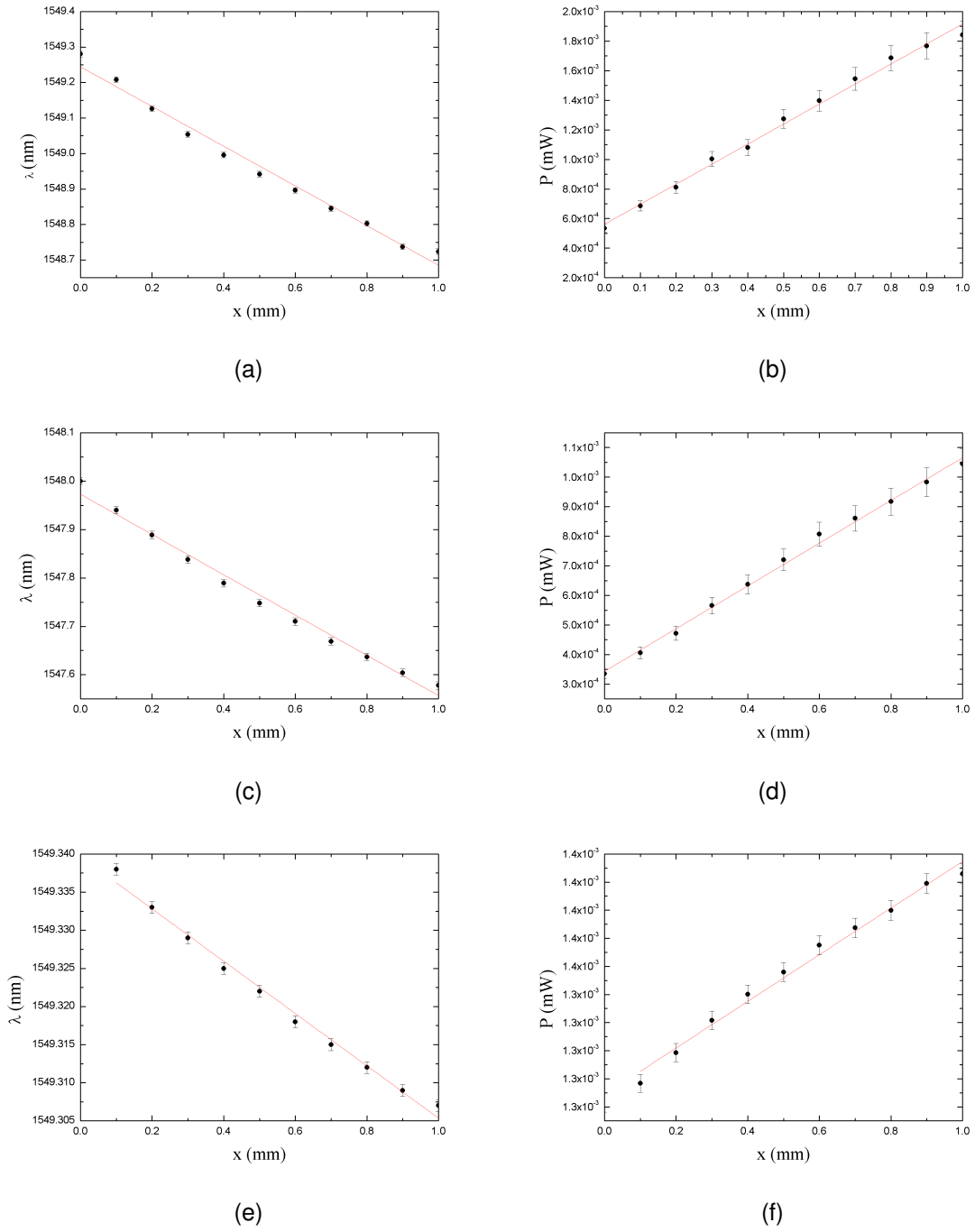

Figure 5.13: Results of displacement characterization for (a,b) first, (c,d) second and (e,f) third printed sensors.

Printed Sensors	*Bragg Wavelength* (pm/mm)	*Optical Power* (mW/mm)
(1)	-559.2 ± 22.75	$1.35 \times 10^{-3} \pm 3.68 \times 10^{-5}$
(2)	-416 ± 16.3	$7.21 \times 10^{-4} \pm 2.08 \times 10^{-5}$
(3)	-34.3 ± 1.16	$1.62 \times 10^{-4} \pm 1.00 \times 10^{-5}$

Table 5.1: Fit results from displacement characterization.

The vibration characterization was accomplished through the application of vibration in cantilever's edge mass, likewise in three sensors. From the displacement characterization results and by performing a correct signal processing, it was possible to obtain the position, velocity and acceleration signals produced by the applied vibration. The period and oscillation frequencies were estimated for all sensors, as well as the maximum value of G. These results are presented on table 5.2.

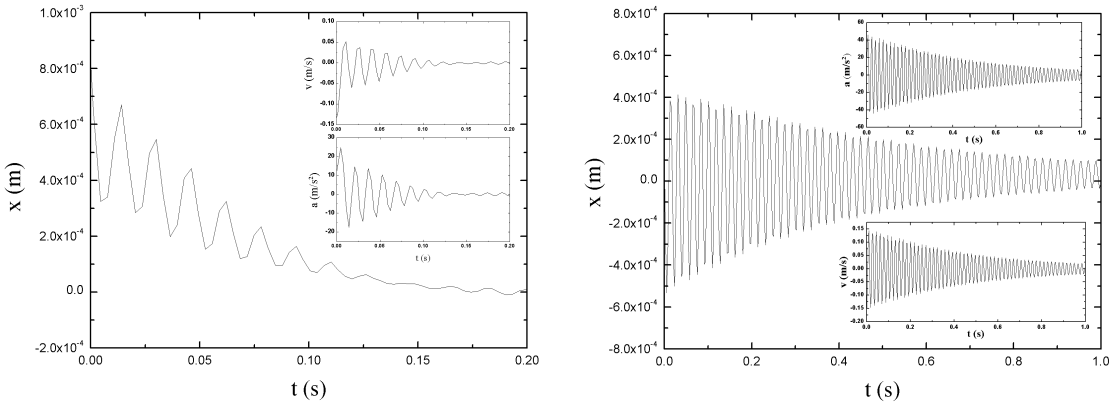

(a) (b)

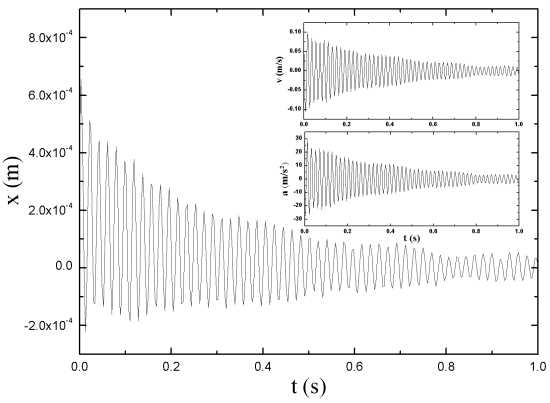

(c)

Figure 5.14: Results of vibration characterization for (a) first, (b) second and (c) third printed sensors.

Printed Sensors	*T (sec)*	*f (Hz)*	*G* (m/s^2)
(1)	0.01667	60	3
(2)	0.01667	60	4.5
(3)	0.01818	55	3

Table 5.2: Determined results from vibration characterization.

For 3D optical fiber accelerometer, an electric analysis was also executed to prove the concept of acceleration variation sensing. For that, the cubic structure presented in figure 5.7(b) was assembled along with the already used tunable lasers, tuned to most sensitive wavelengths of each embedded *FBG*. Following this procedure, it was possible to observe an amplitude variation as the structure was moved. For example, as represented in figure 5.15, after fixing a coordinate system and, by placing one of the sensors as a reference (in this case X-direction), a amplitude variation is observed when the Y and Z directions alter between them. No filter was added to the experimental setup and so, the observable noise is characteristic of the performed measurement.

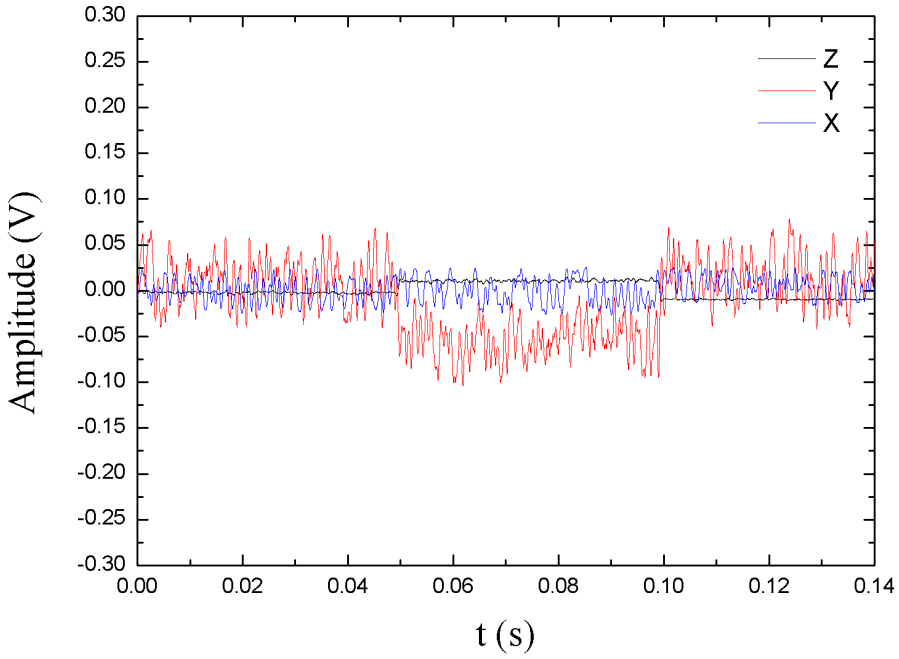

Figure 5.15: Acceleration variation sensing.

5.3 Discussions

The sensing of acceleration variation was achieved with the three configurations explored to assemble an optical fiber accelerometer. All the sensors were produced using the 3D printing technique, proving also how favorable and responsive is the technique. Printed sensors were based on a cantilever structure with *FBGs* embedded in the 3D printed polymer. These sensors together formed the final optical fiber accelerometer, based on a cubic structure. A displacement characterization was accomplished, to evaluate the relation between *Bragg* wavelength and optical power deviation in function of applied displacement, as well as a vibration characterization, so the characteristic position, velocity and acceleration could be determined.

For the 1D optical fiber accelerometer configuration, a sensitivity of $-316.2 \pm 7.2pm/mm$ and $-2.6 \times 10^{-8} \pm 6.2 \times 10^{-10}mW/mm$ was determined in a displacement range of $0.0mm$ to $1.0mm$, with $0.1mm$ steps, evaluating the relation between central wavelength and optical power in function of applied displacement, respectively. From the vibration sensing analysis, it was possible to estimate the period and oscillation frequency, $0.0167sec$ and $60Hz$, approximately. An estimated maximum of $0.15G$ was determined for acceleration measurement. An acceleration variation was registered when the sensor was moved in different directions. This fact demonstrate the previous statement of monitoring movements by registering these variations.

For 2D optical fiber accelerometer configuration, the scaling of printed parts was changed, which reflected in the study of vibration, as expected. Sensitivities of $459.8 \pm 12.82pm/mm$ and $13.5 \pm 0.51pm/mm$ were also determined by a displacement range of $0.0mm$ to $1.0mm$, with $0.1mm$ steps, likewise evaluating the relation between central wavelength and applied displacement, for both printed sensors respectively. The inconsistency in these results is due to the *FBG* positioning during the printing process. An equal analysis was performed to evaluate the optical power behavior in function of displacement. As expected a linear response was registered and, sensitivities of $-4.3 \times 10^{-5} \pm 2.7 \times 10^{-6}mW/mm$ and $3.65 \times 10^{-6} \pm 9.89 \times 10^{-8}mW/mm$ were estimated.

From vibration sensing, it was possible to register oscillation frequencies in the order of $100Hz$, with a period of $0.009sec$ and, an estimated maximum of $1.5G$ and $5G$ for acceleration measurements. These results present a greater oscillation frequency compared to those obtained in 1D configuration. With this structure was again possible to prove the concept of acceleration variation sensing, by demonstrating amplitude variation associated with wrist movement.

The geometry and scaling of the printed parts were again modified for 3D optical fiber accelerometer configuration. These modifications were made in order to keep improving the vibration sensitivity of the *FBG*, aiming for an enhanced response. To the cantilever's edge

was added a rectangular mass and the sensor's characterization begun. As previously, a characterization in displacement was accomplished in a range of $0.0mm$ to $1.0mm$, with $0.1mm$ steps. From this analysis, a linear relation was observed between *Bragg* wavelength in function of displacement and, sensitivities of $-559.2 \pm 22.75pm/mm$, $-416 \pm 16.3pm/mm$ and $-34.3 \pm 1.16pm/mm$ were determined for the three printed sensors. A linear relation was also obtained for optical power, along with sensitivities of $1.35 \times 10^{-3} \pm 3.68 \times 10^{-5}mW/mm$, $7.21 \times 10^{-4} \pm 2.08 \times 10^{-5}mW/mm$ and $1.62 \times 10^{-4} \pm 1.00 \times 10^{-5}mW/mm$. From vibration characterization, similar results were obtained for the three printed sensors. An oscillation frequency of $60Hz$, which corresponds to a period approximately of $0.017sec$ and, a maximum of $4.5G$ for acceleration evaluation. Also, with this configuration, the concept of detecting movements was proved by an amplitude's variation study, after fixing a reference axis and coordinate system.

The assembled sensors endure the performed tests without compromising the optical sensor embedded or its response, promoting their protection and application to hostile environments. The cantilever structure, as previously studied, presented a good response to the performed tests and provided a structure to promote the sensitivity of optical embedded sensor.

Chapter 6

Final Conclusions and Future Work

This dissertation focused on the development of two optical fiber sensors with a 3D printed housing, mainly an optical fiber pressure sensor and an optical fiber accelerometer. The optical sensor implemented in both configurations was a *FBG*, due to its sensitivity and well-known behavior. The cantilever structure was also validated to work as the sensing part of the final configuration. Focusing on sensor's housing, the 3D printing technique was selected, because it allows a flexible design, which can be adapted to the requested application. Considering the biomedical field, this advantage is highly valuable, especially if the monitoring, of a certain bone/organ, is necessary in the body [42]. The proposed housing method is a mutable method, that can be adapted to each location and body. Pursuing this possibility of adapting the sensors to each application, an optical fiber accelerometer and an optical fiber pressure sensor were assembled and tested, in order to prove the concept of pressure and acceleration sensing by the embedded *FBG*. The main objectives of this thesis were accomplished. The developed optical sensors were able to sense pressure and acceleration variation, as expected, without compromising their performance.

The pressure sensor was studied in three different configurations, and finally the three cantilever structure was chosen to function as sensing part, due to the uniform distribution of applied deformation in all three cantilevers. After the printing process, the sensor was calibrated and, a pressure and a vibration characterization were performed. The pressure characterization was executed in a range of $[0, 5]kPa$, low pressures compared to those tested in the available literature [48, 49], but suitable for the desired application. A linear relation was obtained, as expected, between *Bragg* wavelength and applied pressure, presenting a sensitivity of $178pm/kPa$ with a resolution of $0.092kPa$ and, a measurement error of $0.013kPa$.
The vibration characterization was performed for low frequencies: $5Hz$, $2.5Hz$ and $1.5Hz$. And, despite some noise inherent to interrogation system, the pressure sensor was able to

reproduce correctly the tested frequencies. The chosen structure to assemble the optical fiber pressure sensor withstood all tests without compromising the optical sensor or damage the printed structure.

The optical fiber accelerometer was also studied and assembled in three different configurations: 1D, 2D and 3D. Again, the cantilever structure was chosen to function as sensor's head. The final accelerometer was conceived in a cubic structure, dimensionally thought to be manipulated by a human hand, allowing to monitor some movements, particularly the wrist movement. The three configurations were characterized in displacement and vibration. Afterwards, the concept of acceleration sensing was proved by assembling the cubic structure and, by registering a signal amplitude variation caused by a change in acceleration. For each configuration (1D, 2D and 3D), the corresponding number of sensors was printed and characterized. So, for 1D optical fiber accelerometer only one part of the cubic structure was printed with an embedded *FBG* in a cantilever configuration. With this embedded grating, a period of $0.0167sec$ and an oscillation frequency of $60Hz$ were estimated through a vibration characterization. A sensitivity of $-316pm/mm$ and $-2.6 \times 10^{-8}mW/mm$ was determined through the displacement characterization.
For 2D optical fiber accelerometer two sensors were printed with two embedded gratings, respectively. And, both were characterized in displacement and vibration as well. The maximum sensitivity achieved while performing the displacement analysis was $459.8pm/mm$ and $-4.3 \times 10^{-5}mW/mm$. All relations were linear, as expected. The estimated period and oscillation frequency were similar for both sensors, $0.009sec$ and, approximately, $111Hz$.
In order to assemble the 3D optical fiber accelerometer, three sensors were printed, each one with an embedded *FBG*. All three were characterized in displacement and vibration, as the previous ones. Concerning the displacement analysis, the maximum sensitivity achieved was of $-559pm/mm$ and $1.35 \times 10^{-3}mW/mm$. And, similar results for the three sensors were obtained regarding vibration characterization, a period of $0.017sec$ and an oscillation frequency of $60Hz$.
The concept of acceleration variation sensing was proved, since all the assembled configurations responded to a difference in acceleration, that was register as a signal amplitude deviation.

All the printed structures endured the performed tests without compromising the grating structure and its response or damage the housing, which validates the developed design and concept, as well as the chosen technique to create the sensors, 3D printing technique. This work has left some unexplored topics, but provided relevant developments on sensor's housing, allowing its implementation on environments with specific and hostile characteristics. To continue this work particular topics must be addressed:

- Study the developed sensors by implementing them in an hospital or clinical environment:
  - Test the accelerometer in patients that are recovering from strokes or patients suffering from Parkinson's. To monitor their movements and their improvements, in order to evaluate their treatment.
  - Test the pressure sensor as a heart rate sensor, and assess the possibility of reproducing the aortic pulse.
- Explore diverse optical fiber sensors, embedding them through the 3D printing technique.

- Design and 3D Printing Technique:
  - The selected design of the sensors was studied, especially according the desired biomedical application, but new ones should be tested. Investigate if the grating response is enhanced in a different configuration.
  - Test distinct printing methods and materials. And, assess how and how much, different methods and materials influence the sensor's response.
- Fully characterize the embedded grating in temperature, to evaluate the printing material influence on the sensor's response.

Appendix A

Cantilever Structure

The cantilever structure was studied before being implemented on both sensors previously presented. Two structures, with different dimensions, were printed in order to test the cantilever structure. Especially to evaluate how the polymer could influence the sensor's response, since it would act as sensor housing.

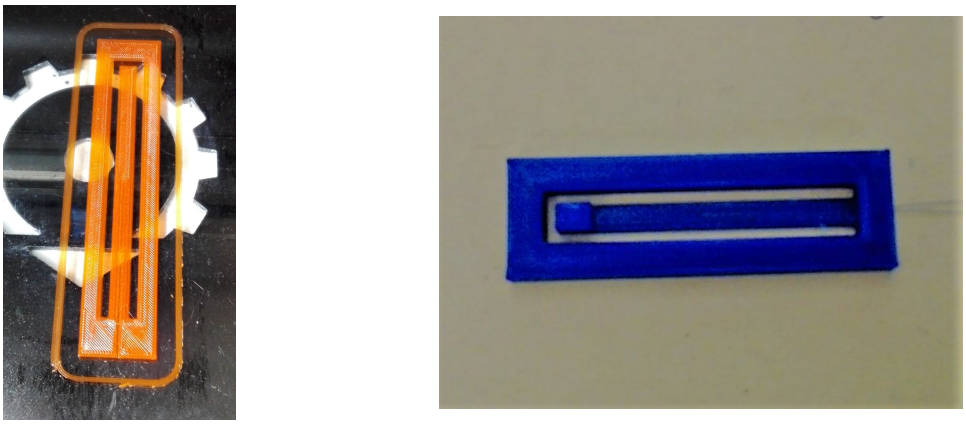

(a) (b)

Figure A.1: Two cantilevers shaped sensors, printed with embedded *FBGs*.

As it can be seen from the figure, the optical sensor was embedded together with the coating, which improves sensor's resistance by strengthening the breakpoint (interface between polymer and optical fiber). Both embedded *FBGs* had a central wavelength of $1550nm$ and $1mm$ length. In the first test, a rectangular shaped sensor was printed (figure A.1(a)), with $20 \times 100 \times 3mm$ dimensions. A central cantilever geometry was designed, with $5 \times 78 \times 1mm$, to host the optical sensor. This sensor was characterized in displacement, temperature and vibration. The second printed sensor was also rectangular shaped with a central cantilever structure (figure A.1(b)), however an additional mass was added to the

cantilever's edge, to improve the vibration sensing. The rectangular structure dimensions are $10 \times 50 \times 3mm$, a central cantilever with $2.50 \times 39 \times 0.5mm$ and an edge mass with $2.50 \times 10 \times 2.50mm$. A characterization in displacement and vibration was performed.
The printing method used was Fused Deposition Modeling (FDM) and the printing material was a thermopolymer, PLA. The sensors were interrogated in reflection and, the experimental setup assembled was composed of a broadband source with a bandwidth of $100nm$, an optical spectrum analyzer (OSA) and an optical circulator. The *Bragg* wavelength shift after the printing process was evident, however through this knowledge it is possible to calibrate the sensor.
The sensor presented in figure A.1(a) was first tested in displacement with the help of a translation stage, from $0.0mm$ to $5.0mm$, with steps of $1mm$. The displacement was applied in the sensor's midpoint and end point (figure A.2(a)), upwards and downward, to contract and stretch the grating in both directions.

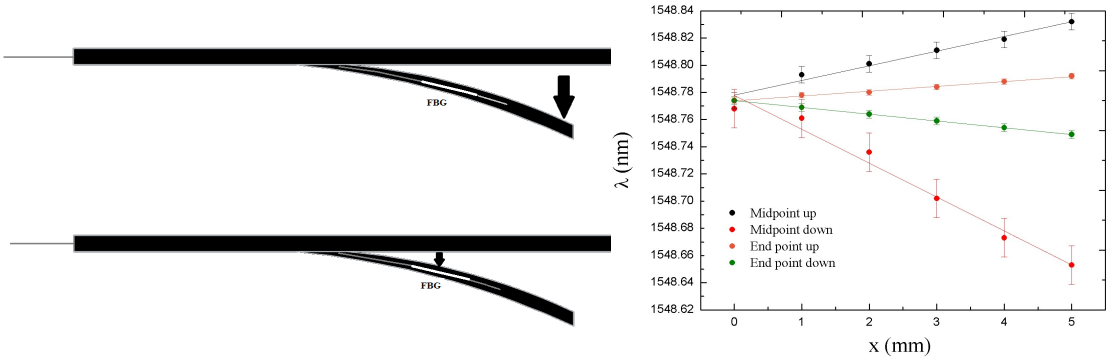

(a) Displacement application point.

(b) Results of displacement characterization.

Figure A.2: Displacement characterization.

Both displacements have linear responses. For midpoint displacement the maximum sensitivity achieved was $10 \pm 0.76pm/mm$ upwards and $20 \pm 1.0pm/mm$ downward. For end point displacement the sensitivity achieved was $3.5 \pm 0.15pm/mm$ upwards and $5 \pm 1pm/mm$ downward.Considering this evaluation, it was concluded that the end point was the most advantageous to apply the deformation, because it causes greater tension at the interface between the cantilever and the surrounding structure. Temperature characterization followed, from $73.5^{o}C$ to $38.9^{o}C$, using an oven. The *Bragg* wavelength was registered in function of temperature during the cooling process. In figure A.3, the results from temperature characterization are presented and, it is possible to observe that the result fits in a polynomial response. This was expected due to the polymeric housing of the sensor. However, in the range of $[38.9, 48.9]^{o}C$ the relation between wavelength and temperature fits in a linear response, with a determined sensitivity of $30 \pm 1pm/^{o}C$.

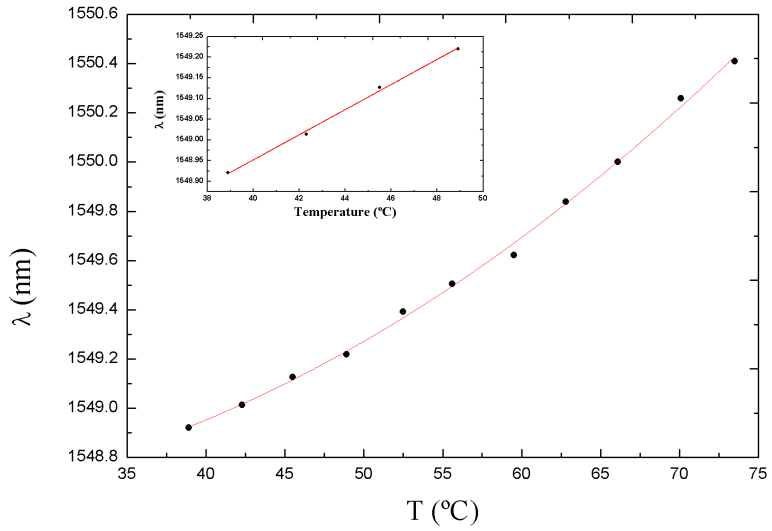

Figure A.3: Temperature characterization.

The last characterization performed with this sensor test was measurements in vibration. The sensor is most sensitive in specific wavelength ranges as it is possible to observe in figure A.4(a). Thus, fixing the most sensitive wavelength and placing a $4g$ weight on cantilever's edge, the effects of vibration were registered in function of time

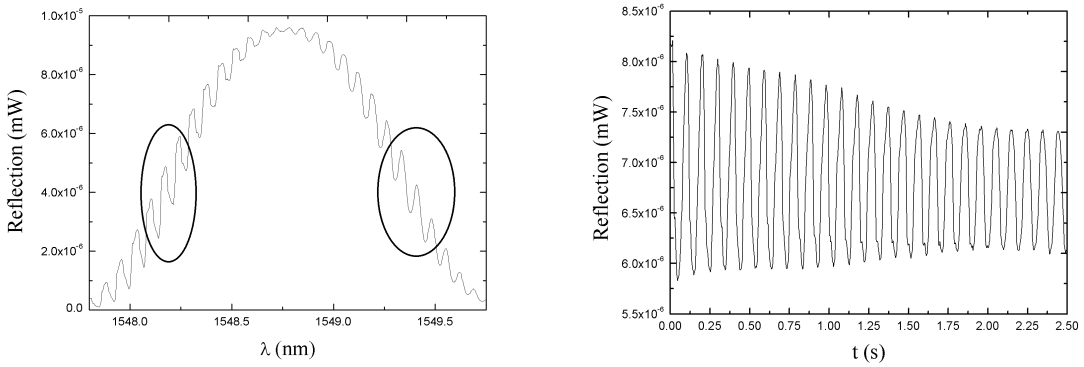

(a) Vibration effects.

(b) Result of vibration characterization.

Figure A.4: Vibration characterization.

The vibration characterization result was recorded during a period of $2.6sec$, from that the oscillation frequency was estimated, $10.2Hz$. From this analysis, it was possible to assess how the sensor response was affected by the polymeric housing and, test the sensor's resistance, improved also due to the housing.

Regarding the second test sensor, as referred before a displacement and vibration characterization was performed. This sensor as a detail that distinguishes it from the previous one, it has two *FBGs* embedded in cantilever structure. One was placed at the cantilever's neutral axis, which means that the optical sensor can't sense any deformation (it was working as a dummy fiber) and, another on the most distant layer from the neutral axis, which has the greatest sensitivity.
Displacement characterization was performed by applying displacement from $0.0mm$ to $1.0mm$ with steps of $0.1mm$, upwards and downward, also with the intent of contract and stretch the *FBG*. During this characterization, the behavior of both embedded *FBGs* was registered and the result is displayed in figure A.5.

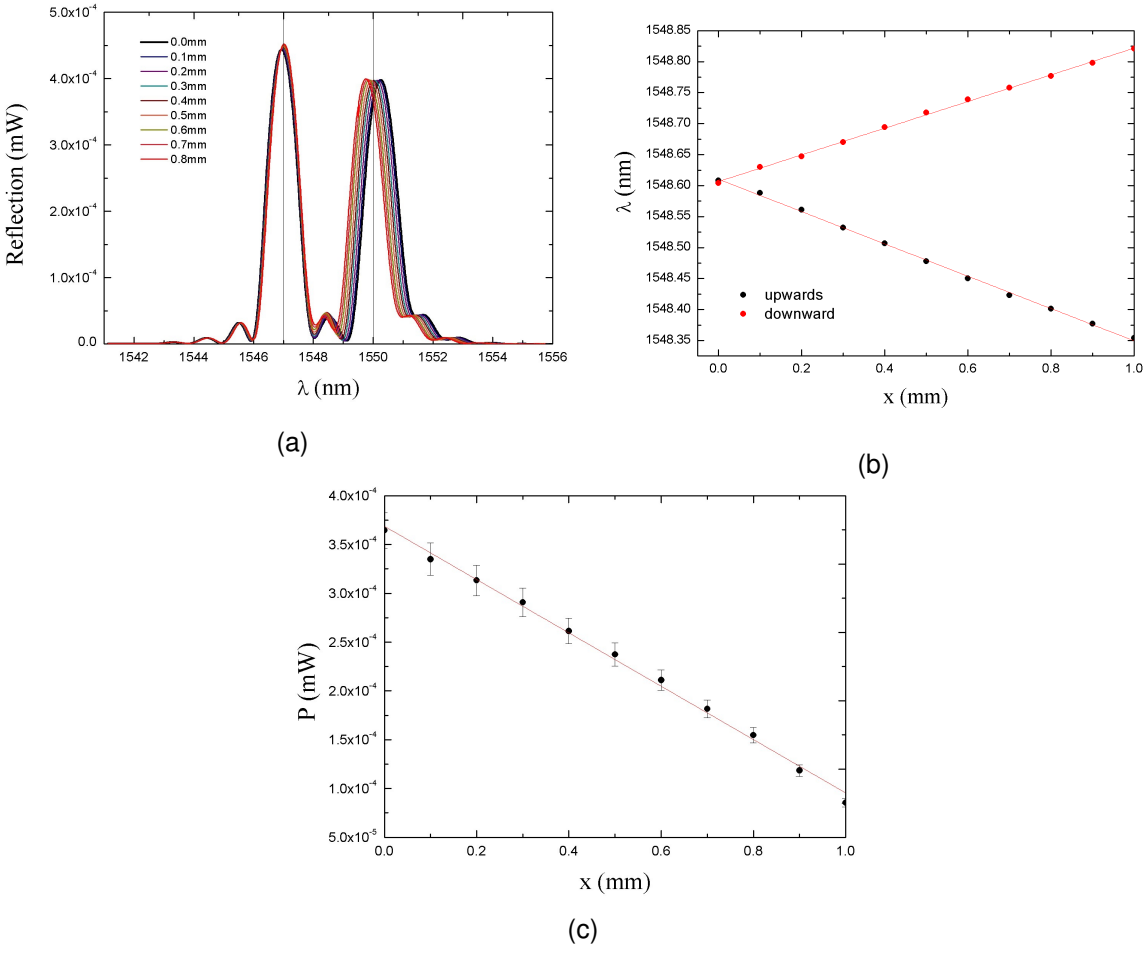

Figure A.5: Displacement characterization: (a) *Bragg* wavelength shift during displacement characterization, dummy fiber on the left, (b) Wavelength shift in function of displacement and (c) Optical power in function of displacement.

From the result presented in figure A.5(a), it is evident the presence of two gratings, as well as the sensing difference between them. The relation between *Bragg* wavelength and applied displacement is presented on figure A.5(b) and given the linear relation, a linear fit was executed, leading to sensitivities of $215 \pm 2.36 pm/mm$ downward and $-260 \pm 3.05 pm/mm$ upwards.

The vibration characterization was performed by applying vibration to cantilever's edge. From that and together with the optical power result, it was possible to determine the position, velocity and acceleration characteristics of the applied vibration. Period and oscillation frequency were also estimated, respectively, $0.009 sec$ and $111 Hz$.

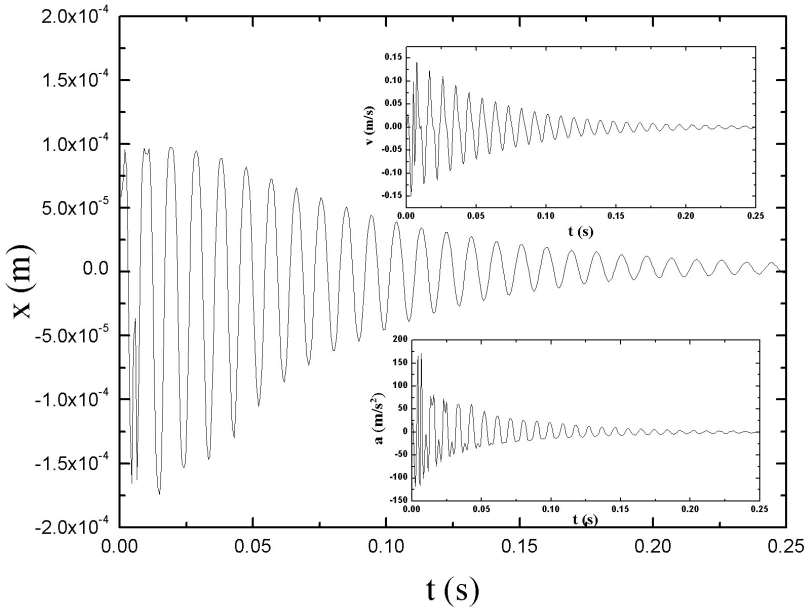

Figure A.6: Vibration characterization.

The optical sensor's response wasn't compromised due to the introduction of polymeric housing, which improved sensor's protection and its applicability in harsh environments. From this test, the cantilever structure was validated and, proved to be an advantageous configuration to implement and host the optical elements.

Appendix B

Optical Fiber Pressure Sensor: Design and Simulations

Different designs were tested for the final structure of the optical fiber pressure sensor. The cantilever structure, as said before, turned out to be an advantageous configuration to implement together with *FBGs*, due to their working principle. Thus, it was implemented as the sensing part of the pressure sensor. The final pressure sensor structure could be assembled with multiple support sites, corresponding to the contact sites between the sensor head and its base. Three different arrangements were simulated on Solidworks by applying deformation on the designed part, to assess which should be implemented. The final configuration was chosen based on the uniformity of the deformation applied in all the cantilevers. A designed part with two, three and four cantilevers was tested in strain and, the obtained results for the two and four cantilevers configuration are presented above.

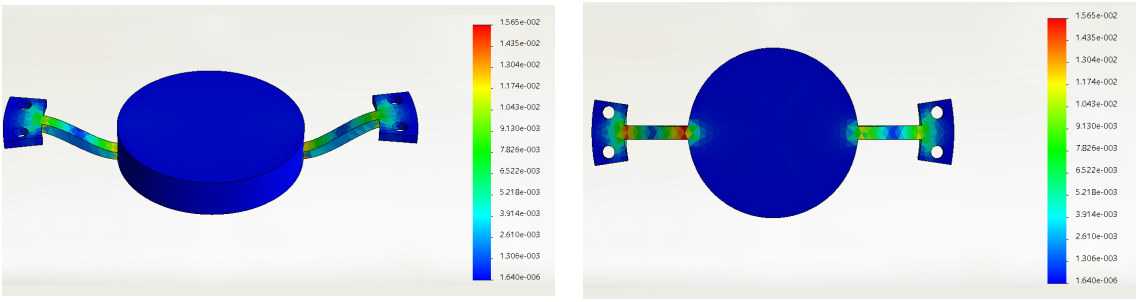

(a) (b)

Figure B.1: Strain simulation results for two cantilever structure: (a) frontal view and (b) bottom view.

Through the simulation results, it is obvious that the applied force is non-uniform in the two cantilevers, thus the *FBG* response to applied deformation would depend on which cantilever it is embedded. The same happened with the four cantilevers structure, which revealed a non-uniform behavior under applied deformation, as it can be seen in the results presented on figure B.2.

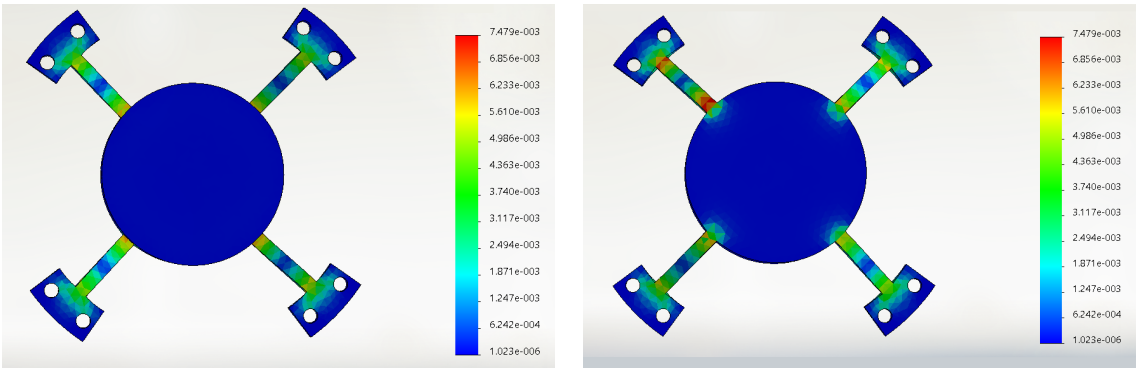

(a) (b)

Figure B.2: Strain simulation results for four cantilever structure: (a) frontal view and (b) bottom view.

The implemented structure to assemble the final optical fiber pressure sensor was the three cantilever configuration. In that configuration, as it can be seen in chapter 4.1., the applied force is uniform in all the three cantilevers, thus the optical sensor response won't depend on which cantilever is placed.

References

[1] Kenneth O. Hill and G. Meltz. Fiber bragg grating technology fundamentals and overview. *Journal of Lightwave Technology*, 15(8), August 1997.

[2] M. F. M. Santos E. Fujiwara and C. K. Suzuki. Flexible optical fiber bending transducer for application in glove-based sensors. *IEEE Sensors Journal*, 14(10), 2014.

[3] A. B. Lobo-Ribeiro J. L. Santos P. Roriz, O. Frazao and J. A. Simoes. Review of fiber-optic pressure sensors for biomedical and biomechanical applications. *Journal of Biomedical Optics*, 18, 2013.

[4] N. Alberto P. Antunes H. Lima P. S. Andre R. Nogueira C. Leitao, L. Bilro and J. L. Pinto. Feasibility studies of bragg probe for noninvasive carotid pulse waveform assessment. *Journal of Biomedical Optics*, 18, 2013.

[5] T.K. Gangopadhyay. Prospects for fibre bragg gratings and fabry-perot interferometers in fibre-optic vibration sensing. *Sensors and Actuators A*, 113:20–38, 2004.

[6] R. E. Jones G. R. Jones and R. Jones. *Optical Fiber Sensor Technology: Advanced Applications - Bragg Gratings and Distributed Sensors*. SPRINGER SCIENCE+BUSINESS MEDIA, LLC, 2000.

[7] Y. Liu W. Zhang L. Zhang B. A. L. Gwandu, X. W. Shu and I. Bennion. Simultaneous measurement of strain and curvature fibre bragg gratings. *Sensors and Actuators A*, 96:133–139, 2002.

[8] Liu Z. Dong X., Liu Y. and X. Dong. Simultaneous displacement and temperature measurement with cantilever-based fiber bragg grating sensor. *Optics Communications*, 192:213–217, 2001.

[9] T. Li Y. Tan, L. Cai and Q. Wei. Study on non-contact fiber bragg grating vibration sensor. pages 13–15, Montreal, Quebec, Canada, August 2014.

[10] M. Hu J. Wang C. Guo S. Wang, Y. Wang and H. Lei. A new style of fbg vibration sensor. *Journal of Basic and Applied Physics*, 2:20–23, February 2013.

[11] Barry Berman. 3-d printing: The new industrial revolution. *Business Horizons*, 55:155–162, 2012.

[12] M. C. van Langeveld C. Schubert and L. A. Donoso. Innovation in 3d printing: a 3d overview from optics to organs. *Br. J. Ophthalmol*, 98:159–161, 2014.

[13] W. Zhang K. Koczur A. Kirsten R. Telle C. Bergmanna, M. Lindner and H. Fischer. 3d printing of bone substitute implants using calcium phosphate and bioactive glasses. *Journal of the European Ceramic Society*, 30:2563–2567, 2010.

[14] S. E. Hudson K. Willis, E. Brockmeyer and I. Poupyrev. Printed optics: 3d printing of embedded optical elements for interactive devices. In *ACM Symposium on User interface Software and Technology (UIST '12)*, pages 589–598, 2012.

[15] Y. Baron R. Sanders E. Sachs A. Lightman C. Hull, M. Feygin and T. Wohlers. Rapid prototyping: current technology and future potential. *Rapid Prototyping Journal*, 1:11–19, 1995.

[16] Paul F. Jacobs. *Rapid Prototyping and Manufacturing: Fundamentals of StereoLithography*. Society of Manufacturing Engineers, 1992.

[17] D. Rosen I. Gibson and B. Stucker. *Additive Manufacturing Technologies: 3D Printing, Rapid Prototyping and Direct Digital Manufacturing*. Springer, 2009.

[18] A. M. Beese and B. E. Carroll. Review of mechanical properties of ti-6al-4v made by laser-based additive manufacturing using powder feedstock. *JOM*, 68(3), 2016.

[19] G. C. Anzalone T. C. Havens P. G. Sanders A. Pinar, B. Wijnen and J.M. Pearce. Low-cost open-source voltage and current monitor for gas metal arc weld 3d printing. *Journal of Sensors*, 2015.

[20] John Tyndall. *Notes of a course of nine lectures on light delivered at the Royal institution of Great Britain*. London, Longmans, 1870.

[21] H. H. Hopkins and N. S. Kapany. A flexible fibrescope, using static scanning. *Nature*, (173), 1954.

[22] Jeff Hecht. *City of Light: The Story of Fiber Optics*. 1999.

[23] M. Borner. Electro-optical transmission system utilizing lasers, 1974.

[24] J. Minowa H. Ishio and K. Nosu. Review and status of waveiength-division-multiplexing technology and its application. *Journal of Lightwave Technology*, (4), 1984.

[25] D. C. Johnson K. O. Hill, Y. Fujii and B. S. Kawasaki. Photosensitivity in optical fiber waveguides: Application to reflection filter fabrication. *Applied Physics Letters*, (32), 1978.

[26] C. Fabry and A. Perot. Sur les franges des lames minces argentees et leur application a la mesure de petites epaisseurs d'air. *Ann. Chim. Phys.*, 12:459–501, 1897.

[27] Charles M. Davis. Fiber optic sensors: an overview. *Optical Engineering*, 24:347–351, 1985.

[28] Heather J. Patrick M. LeBlanc K. P. Koo C. Askins M. Putnam A. D. Kersey, M. Davis and E. Friebele. Fiber grating sensors. *Journal of Lightwave Technology*, 15(8), August 1997.

[29] S. Cinquemania G. Cazzulania and L.Comollia. Enhancing active vibration control performances in a smart structure by using fiber bragg gratings sensors. *Sensors and Smart Structures Technologies for Civil, Mechanical, and Aerospace Systems*, 8345, 2012.

[30] I. Dias L. A. Ferreira O. Frazao, F. M. Araujo and J. L. Santos. Sensores de bragg em fibra optica. In *Jornadas de Engenharia de Telecomunicações e Computadores - JETC99*, pages XI–23–26, 1999.

[31] M. B. Marques H. F. Martins and O. Frazao. Intensity vibration sensor based on raman fiber laser using a distributed mirror combined with bragg grating structures. *Applied Physics B*, 2014.

[32] J. Kiddy C. Baldwin, J. Niemczuk and T. Salter. Review of fiber optic accelerometers. In *IMAC: Conference and Exposition on Structural Dynamics IMAC XXIII*, 2005.

[33] J. D. C. Jones A. S. Gerges, T. P. Newson and D. A. Jackson. High-sensitivity fiber-optic accelerometer. *Optics Letters*, 14(4), 1989.

[34] J. A. Gilbert Wei Su and M. D. Morrissey. General-purpose photoelastic fiber optic accelerometer. *Opt. Eng*, 36:22–28, 1997.

[35] H. Tam B. Guan and S. Liu. Temperature-independent fiber bragg grating tilt sensor. *IEEE Photonics Technology Letters*, 16(1), 2004.

[36] K. Jerzy and P. Ryszard. A cantilever optical-fiber accelerometer. *Sensors and Actuators A*, 68:350–355, 1998.

[37] Q. Jiang and M. Yang. Simulation and experimental study of a three-axis fiber bragg grating accelerometer based on the pull-push mechanism. *Measurement Science and Technology*, 24, 2013.

[38] P. Mendes A. Silva, A. Goncalves and J. Correia. Fbg sensing glove for monitoring hand posture. *IEEE Sensors Journal*, 11(10), 2011.

[39] R. Zheng W. Tao, T. Liu and H. Feng. Gait analysis using wearable sensors. *Sensors*, 12, 2012.

[40] H. Zhou and H. Hu. Human motion tracking for rehabilitation - a survey. *Biomedical Signal Processing and Control*, 3:1–18, 2008.

[41] Eric Pinet. Pressure measurement with fiber-optic sensors: Commercial technologies. In *21st International Conference on Optical Fiber Sensors*, volume 7753, 2011.

[42] J. Potes M. Oliveira O. Frazao J. L. Santos P. Roriz, J. Ferreira and J. Simoes. In vivo measurement of the pressure signal in the intervertebral disc of an anesthetized sheep. *Journal of Biomedical Optics*, 19, 2014.

[43] M. Sugihara O. Tohyama, M. Kohashi and H. Itoh. A fiber-optic pressure microsensor for biomedical applications. *Sensors and Actuators A*, 66:150–154, 1998.

[44] R. Apsari Y.G. Yhun Yhuwana and M. Yasin. Fiber optic sensor for heart rate detection. *Optik*, 134:28–32, 2017.

[45] H. Ugnell L.G.Lindberg and P. A. Oberg. Monitoring of respiratory and heart rrate using a fibre-optic sensor. *Medical and Biological Engineering and Computing*, 30:533–537, 1992.

[46] S. Meaume M. E. Safar, O. Henry. Aortic pulse wave velocity: An independent marker of cardiovascular risk. *The American Journal of Geriatric Cardiology*, 2001.

[47] S. Djane G. M. London J. Blacher, R. Asmar and M. E. Safar. Aortic pulse wave velocity as a marker of cardiovascular risk in hypertensive patients. *The American Journal of Geriatric Cardiology*, 1998.

[48] Q. Zhao Y. Liu L. Liu, H. Zhang and F. Li. Temperature-independent fbg pressure sensor with high sensitivity. *Optical Fiber Technology*, (13):78–80, 2007.

[49] Z. Liu Z. Guo X. Dong K. Chiang Y. Zhang, D. Feng and B. Chu. High-sensitivity pressure sensor using a shielded polymer-coated fiber bragg grating. *IEEE Photonics Technology Letters*, 13(6), 2001.

[50] F. Colpo J. Botsis, L. Humbert and P. Giaccari. Embedded fiber bragg grating sensor for internal strain measurements in polymeric materials. *Optics and Lasers in Engineering*, (43):491–510, 2005.

[51] J. Witt M. Schukar K. Krebber F. Pirotte A. Grillet, D. Kinet and A. Depre. Optical fiber sensors embedded into medical textiles for healthcare monitoring. 8(7), 2008.

[52] Richard F. Tinder. *Relativistic Flight Mechanics and Space Travel*. Morgan&Claypool, 2006.

[53] E. Udd and Jr. W. B. Spillman. *Fiber Optic Sensors: An Introduction for Engineers and Scientists.* Wiley, second edition, 2011.

[54] T. A. Berkoff and A. D. Kersey. Experimental demonstration of a fiber bragg grating accelerometer. *IEEE Photonics Technology Letters*, 8(12), 1996.

[55] Sipus Z. Babic D. Igrec B., Bosiljevac M. and Rudan S. Fiber-optic vibration sensor for high-power electric machines realized using 3d printing technology. *Photonic Instrumentation Engineering III*, 9754, 2016.